TUNABLE MID-INFRARED LIGHT SOURCE BASED ON DIFFERENCE FREQUENCY GENERATION IN PERIODICALLY POLED LITHIUM NIOBATE

TUNABLE MID-INFRARED LIGHT SOURCE BASED ON DIFFERENCE FREQUENCY GENERATION IN PERIODICALLY POLED LITHIUM NIOBATE

By

LING HAN

A Thesis

Submitted to the School of Graduate Studies

In Partial Fulfillment of the Requirements

for the degree

Master of Applied Science

McMaster University

Master of Applied Science (2007) McMaster University

(Engineering Physics) Hamilton, Ontario

TITLE: Tunable Mid-Infrared Light Source Based on Difference Frequency Generation in Periodically Poled Lithium Niobate

AUTHOR: Ling Han B. Sc. (Peking University)

SUPERVISOR: Professor Chang-Qing Xu

NUMBER OF PAGES: Xi, 81

ABSTRACT

In this work, tunable Mid-Infrared (IR) light sources based on quasi-phase matched (QPM) difference frequency generation (DFG) by periodically poled lithium niobate (PPLN) crystals are studied. The theory of DFG and the characteristics of lithium niobate crystals are described and analyzed. Characteristics of the wavelength tuning of QPM DFG by PPLN crystals are studied. In order to analyze in detail, simulation and experimental data of the widely tunable mid-IR laser source around 2 μm to 5 μm wavelength are presented. The simulations of DFG process by PPLN are conducted based on the nonlinear optics reported. In the experiment, a 1.064 μm Nd:YAG laser and a tunable Ti:sapphire laser are employed as the signal and pump lasers, respectively. Based on the studies of the wavelength tuning characteristics at different temperatures, an optimization procedure to achieve a maximum wavelength tuning range is proposed. The potential applications in gas detection of the mid-IR source are also described briefly. Recommendation for future works and potential applications of the PPLN DFG based mid-IR lasers are discussed.

Acknowledgement

First of all, I would like to thank Dr. Chang-Qing Xu sincerely, who has been my supervisor at McMaster University, for the past two years. Dr. Xu has devoted a lot of time and attention to supporting me throughout my academic pursuits. He has been always patient providing valuable help and advice, even when I'm not doing very well with the project. I owe my studies and academic career to him. Then, I would like to thank all the members in my group for their continual support and nice help on this project. Without their experimental and analytical help this project would not have been done. Also, I would also like to thank the other members of my defense committee: Dr. Xun Li and Dr. Jen-Shih Chang for taking their time with this thesis.

I owe special thanks to the excellent people I have worked with. Without their continual support this project could not have progressed to the point it has today. I am especially grateful to Dr. Wanguo Liang for his extensive efforts in sample preparation and his nice advice. I am also very grateful to Dr. Yong Wang for his continuous useful guidance. I also have to thank Dr. Xiao-ming Gao from Laboratory of Atmospheric optics, Anhui Institute of Optics and Fine Mechanics, China, for his experimental guidance and valuable suggestion in the process of cooperation.

TABLE OF CONTENTS

List of Tables

List of figures

CHAPTER 1: INTRODUCTION

1.1 Background

Mid - infrared spectrum region is the range from about 2 μm to 20 μm in the spectroscopy. In recent years, mid-IR lasers have attracted much attention for their potential use in various applications, such as fiber-optics chemical sensors, biomedical technology, high-resolution spectroscopy, and particularly, environmental monitoring [1-6] where they are important sources for trace gas detection [3-6].

Many trace atmospheric gas species have optical absorption bands in the mid infrared region, because most molecules have fundamental vibrational absorption lines in the infrared wavelength region of 2 - 5 μm. Thus, laser absorption spectroscopy is considered to be the most effective technique to detect these trace atmospheric gases. Each type of molecule has its own spectral signature with narrow absorption lines and can hence be reliably identified with high precision. Therefore, a broadly tunable mid-IR laser source is very desirable.

As far as we know, there are several methods to generate mid-infrared lights, including antimonide diode lasers, quantum cascade technology, lead-salt tunable diode lasers, tunable solid-state lasers and wavelength conversion techniques. Among the reported mid-IR light generation techniques, those based on difference-frequency generation (DFG) in periodically poled lithium niobate (PPLN) or other nonlinear

optical crystals have attracted special attention due to the attractive combination of broad wavelength tunability and sharp linewidth.

1.2 Research Motivation

As far as we know, light generation by the quasi-phase matching (QPM) DFG process in nonlinear crystals, especially lithium niobate, is one of the most effective way to achieve mid-IR radiation for trace gas detection applications. Broadly tunable mid-IR light source, which can monitor variety of trace atmospheric gases, based on single device of nonlinear optical crystal is very desirable. In recent years, there are large amount of works reported on this topic which has attracted much interest. For example, a tuning range of 5 - 12 μm has been achieved using difference-frequency mixing in a $AgGaS_2$ crystal [7]. By using a PPKTP crystal as the DFG medium in an optical parametric oscillator (OPO), mid-IR generation from 4.5 to 4.6 μm has been achieved when the temperature was tuned from 25 °C to 200 °C [8]. DFG in PPLN crystals is particularly interesting because of its high conversion efficiency, wide thermo-optic tuning range, and high transparency in the entire 2 - 5 μm region. In Ref. 9, light generation from 4 - 4.6 μm has been achieved in a PPLN crystal by varying the temperature from 16 °C to 40 °C while simultaneously tuning the Ti^{3+}:sapphire laser (812 - 835nm) and fixing a diode laser wavelength of 1020 nm. In Ref. 10, a bandwidth of ~ 100 nm has been achieved by setting the temperature around 26 °C in a multisection temperature-tuned PPLN device. Despite the prospect of achieving

broad band mid-IR generation, these examples illustrate that the exact generation process in PPLN and/or other crystals is not yet fully understood, with questions such as why the reported tunable bandwidths are so different and how to achieve the maximum tunable bandwidth from a single device remain unanswered.

In this work, the research object is to demonstrate a widely tunable mid-IR laser source, generated by the QPM DFG process in PPLN crystal. While tuning the input wavelength of pump laser and operation temperature of single PPLN, very broad tunable mid-IR light, which spans the spectral region from 2 to 5 μm for detection of different species of trace gas, such as CH_4, CO_2, SO_2, C_2H_2, H_2CO, N_2O, can be achieved. It's worth noting that for H_2CO and N_2O, there are not yet commercial detectors on the market, which makes this mid-IR light a good source for the detection of these two types of gas.

In chapter 2, an introduction of mid-IR light sources is presented. And a comparison of main characteristics of different types of mid-IR lasers, including antimonide diode laser, quantum cascade laser, lead-salt diode laser and tunable solid-state laser, is demonstrated. Then, frequency conversion methods to generate mid-IR light are presented and the main characteristics are introduced. DFG process, as the most important way to achieve mid-IR laser, is also briefly discussed in this chapter.

In chapter 3, the basic theory and principles of DFG are summarized. Fundamental equations, concepts, parameters, and main characteristics are discussed.

Chapter 3 also gives an overview of the characteristics of lithium niobate crystal. Its structure, nonlinear properties and applications are presented. Periodically poled

lithium niobate (PPLN) crystal for quasi-phase matching is discussed. Then the electric-field poling technique to fabricate PPLN is also briefly described.

Chapter 4 demonstrates the experiment setup of QPM DFG in PPLN crystals. In the experiment, the signal and pump laser sources are a CW Nd:YAG laser at 1.064 μm. and a CW tunable Ti:sapphire laser tunable from 780 nm to 880 nm, respectively. A broadly tunable mid-IR source is provided and used in the application of atmosphere gas detection.

In chapter 5, wavelength tuning of mid-IR lasers based on DFG in a single PPLN crystal has been simulated theoretically for the use of atmospheric trace gas detection. In this simulation process, the signal and pump laser sources are assumed to be a CW Nd:YAG laser at 1.064 μm. and a CW tunable Ti:sapphire laser tunable from 780 nm to 880 nm, respectively, which are the same as the experiment. An optimization procedure to achieve the maximum tunable bandwidth from a PPLN crystal with a fixed period, when the wavelength of signal laser and operational temperature are tunable, has been proposed

In chapter 6, a conclusion of all the works is made and possible future works and applications are discussed.

CHAPTER 2:

MID-IR LASER SOURCES AND APPLICATIONS IN SPECTRASCOPY

2.1 Direct mid-IR laser sources

Mid - infrared spectrum region is the range from about 2 μm to 25 μm in the spectroscopy. Lasers in this region have many practical and potential applications in environmental monitoring [1]. Therefore, mid-IR lasers have attracted many attentions around the world these years.

There are several different methods to generate mid-infrared lights. Fig. 2.1 shows the spectral coverage of the reported laser sources in the mid-IR wavelength region [2]. These sources can be divided into two types, class "A" and "B". Class "A" are laser sources which generate CW mid-IR lasers directly from gain in gas discharge, semiconductors, rare-earth and transition-metal doped solid-state bulk materials or optical fibers. Class "A" sources include CO laser, CO2 laser, lead salt laser and so on. Class "B" are laser sources based on frequency conversion techniques, including difference frequency generation (DFG), optical parametric oscillator (OPO), and optical parametric amplifier (OPA), in nonlinear optical materials. As shown in Fig. 2.1, many non-linear optical crystals, such as $LiNbO_3$, $KTiOPO_4$ (KTP), $KTiOAsO_4$, $AgGaS_2$ and so forth, have been used for this purpose.

The advantages of class "A" mid-IR laser sources, which are the direct laser sources, are inherently more compact, and class "B" laser sources can be made to be tunable over a much wider wavelength range in mid-IR spectroscopy, which is an important advantage for certain applications.

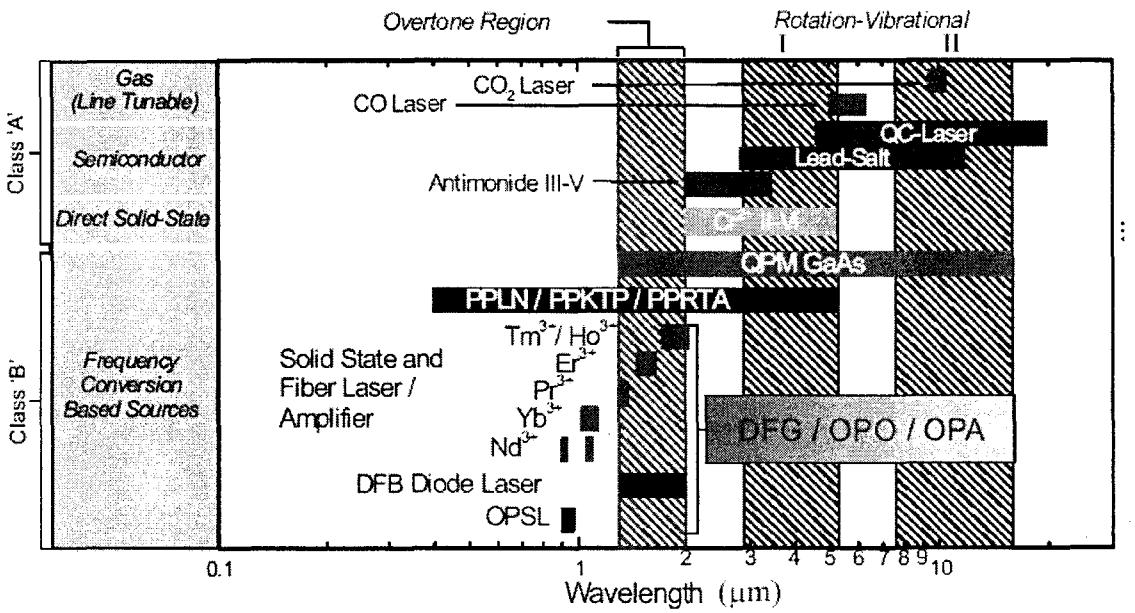

Fig. 2.1 Laser sources and typical wavelength coverage. The wavelengths of the two atmospheric windows I (2.9–5.3 μm) and II (7.6-16 μm), which are typically accessed for trace gas detection [2]. Here DFG means Difference Frequency Generation, OPO means Optical Parametric Oscillator, OPA means Optical Parametric Amplication.

In the following sections, several types of reported mid-IR lasers are briefly described and the advantages and disadvantages of each type of mid-IR lasers are also summarized.

2.1.1 Antimonide Diode Laser Sources

First of all, radiations in the mid-infrared region can be produced by antimonic diode lasers [3]. By using structures grown by molecular beam epitaxy on GaS substrates and strained GaInSbAs quantum wells between Ga(Al)Sb(As) barriers in the active region, continuous wave (CW) lasing at room temperature at wavelengths above μm can be achieved. These laser sources emit light in a fundamental spatial mode and could exhibit single frequency operation at different currents and temperatures. Their spectral regions cover the absorption lines of a large number of different types of gases in atmosphere, including CH_4, CO, NH_3 and NO_2. There are several research groups trying to extend the wavelength coverage of these antimonide diode lasers to the fundamental spectral region of the typical gas molecules. Antimonide diode lasers in the 2 to 3 μm spectral range and InAsSb/InAs lasers in the 3 to 5 μm spectral range have been demonstrated. However, the main disadvantage of these lasers is that these devices must be operated in an external cavity configuration to achieve stable and narrow-linewidth operation. Besides, reliable single-frequency operation requires cryogenic cooling, although room-temperature operation has already been demonstrated. Table 2.1 shows the summary of the characteristics of antimonide diode laser described above.

Table 2.1 Summary of antimonide diode laser characteristics

Wavelength range (μm)	Tuning (coarse/fine)	Power (mW)	Linewidth	Beam profile characteristics	Operating requirements
2-3 & 3-5	1-2 cm^{-1}	0.1 (single-mode)	50 MHz	Elliptical Astigmatic Highly divergent	Thermoelectric(2-3μm) Cryogenic cooling (> 3μm)

2.1.2 Tunable Solid-State Lasers

Tunable solid-state lasers have also been reported to achieve mid-IR light. A solid-state laser is one that uses a crystal, whose atoms are rigidly bonded, unlike a gas. The crystal produces laser light after light is pumped by either a lamp or another laser. A major and important class of tunable lasers is based on the vibration broadened transitions that can occur in certain gain media, such as color centers and certain transition metal or rare-earth ions in crystalline hosts [4 - 6]. Stimulated emission can be made to occur at any desired frequency within the region of the emission band, when the laser medium is placed in a tunable cavity and pumped above laser threshold. Figure 2.2 shows the typical diagram of tunable solid-state laser. Tunable laser media based on 3d-3d transitions of transition-metal ions and 4f-5d transitions of rare-earth ions cover the mid-infrared spectral range between 1 μm to 4.7 μm.

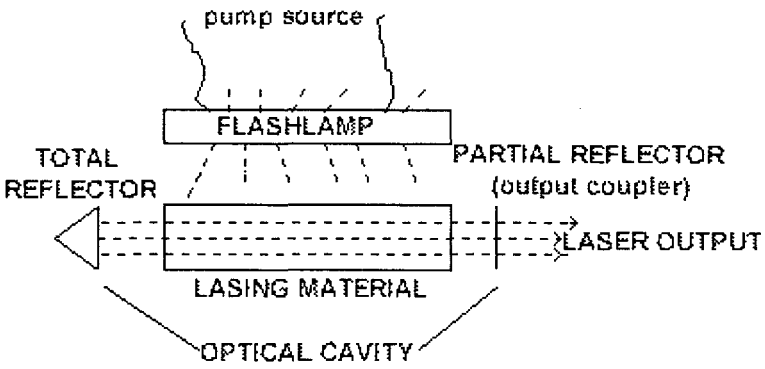

Fig. 2.2. Typical scheme of Solid State Laser

Tunable solid-state lasers acting as mid-IR sources have several advantages, including room-temperature operation, broad tunability, the possibility of direct diode-pumping, erbium fiber amplifier and CW operation. Table 2.2 demonstrates the summary of the characteristics of tunable solid-state laser.

Table 2.2. Summary of tunable solid- state laser characteristics

Wavelength range (μm)	**Tuning (coarse/fine)**	**Power (mW)**	**Linewidth**	**Beam profile characteristics**	**Operating requirements**
2-5	600 nm/ 1 cm^{-1}	200-1000 20	800MHz, 1s 0.1MHz, 1s	TEM_{00} Cavity subject to pointing instability	Low technical noise environment

2.1.3 Quantum Cascade Technology

Min-IR light can also be generated by quantum cascade (QC) technology, which was first demonstrated in 1994 [7]. The basic concept of QC lasers is a periodic repetition of active sections and so-called injection regions, in which a miniband is formed. A typical structure is shown in Fig. 2.3. From the injector miniband the electrons are injected into the upper laser energy level 4 of the active section. Here the laser transition takes place. After that, the lower laser energy level 3 is emptied by LO-phonon emissions and the electrons enter the next stage through tunneling. A quantum-cascade laser is based on intersubband-transitions of electrons inside a quantum-well structure. Therefore, unlike other semiconductor light sources, the emitted wavelength is not determined by the band gap of the used material but on the thickness of the constituent layers.

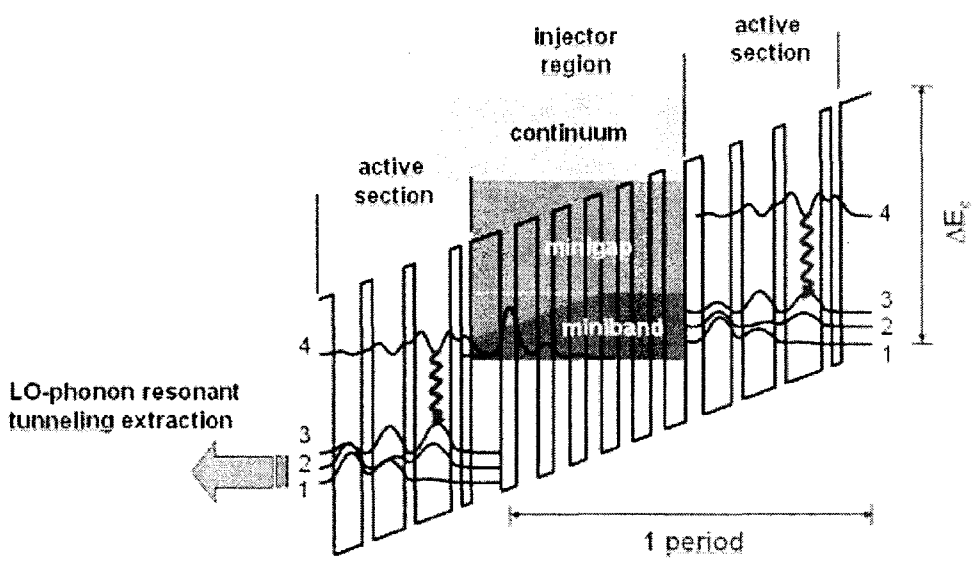

Fig. 2.3 Typical structure of a quantum cascade laser

The wavelength of a quantum cascade laser depends on the thickness of the quantum well and barrier layers of the active region, and they can operate both as CW and pulsed

lasers [8, 9]. But the problem is that their tunable regions are limited, which can't satisfy the needs of practical applications. And, they have to be operated at very low temperatures. Table 2.3 summarizes the quantum cascade laser characteristics.

Table 2.3 Summary of quantum cascade laser characteristics

Wavelength range (μm)	**Tuning (coarse/fine)**	**Power (mW)**	**Linewidth**	**Beam profile characteristics**	**Operating requirements**
4.3-24	35 cm^{-1} with external grating cavity/ 3 cm^{-1}	1-100 (CW, single frequency) 50 (pulsed)	0.001-10 MHz, CW >150 MHz, pulsed	Elliptical Astigmatic Highly divergent	Cryogenic cooling (CW) Peltier cooling (pulsed) High voltage, high current low noise driving electronics

2.1.4 Lead-Salt Tunable Diode Lasers

Lead-salt tunable diode lasers are another type of sources to generate mid-IR light [10]. Lead-salt diode lasers have been developed for operating at wavelengths from 3 to 30 μm and have been available since the mid-1960s. These lasers are comprised of PbTe, PbSe, and PbS and various alloys of these compounds with the same materials above and with SnSe,SnTe,CdS and other materials. Diode lasers have so many merits, such as compact size, relatively high efficiency, narrow bandwidth and reliability. Any given

device can be actively tuned in wavelength over ~ 100 cm^{-1} by changing the device temperature, or over tens of cm^{-1} by changing the injection current.

But they have some obvious operational drawbacks such as their inherent requirement of cryogenic cooling and limited single frequency wavelength coverage. Lead-salt diode lasers also exhibit large beam divergence and astigmatism, which places critical and stringent alignment requirements on the collection optics, particularly for the first optical element, which is placed in front of the dewar. Subtle changes in the alignment between the laser and the first collection optic, due to small mechanical changes in the position of either the laser or the optical element, necessitates periodic adjustments to the first collection element, and this may add some mechanical instability to the alignment. Such instability, even when relatively small, in turn often leads to optical noise in IR absorption systems. This noise source, which is produced by unwanted scattering from various optical elements, results in a periodically undulating background structure of varying amplitude, spacing, and temporal frequency.

Despite these drawbacks of lead-salt diode lasers, spectrometers employing these sources still yield excellent sensitivity, even in rugged field environments. Table 2.4 shows the summary of the lead-salt diode laser characteristics.

Table 2.4. Summary of lead-salt diode laser characteristics.

Wavelength range (μm)	**Tuning (coarse/fine)**	**Power (mW)**	**Linewidth**	**Beam profile characteristics**	**Operating requirements**
3-30	100 cm^{-1} / 1-2 cm^{-1}	0.1-0.5	1-1000 MHz	Elliptical Highly astigmatic Highly divergent	Cryogenic cooling

2.2 Frequency Conversion Techniques

Another important method to generate mid-IR radiation is wavelength conversion technique in nonlinear materials, such as Optical Parametric Oscillation (OPO) [11-13], Optical Parametric Amplifier (OPA) and Difference Frequency Generation (DFG). These laser sources are called class "B" type mid-IR laser.

2.2.1 Difference Frequency Generation (DFG)

When two beams of light with different frequencies are induced into a nonlinear optical material, a beam of light with the frequency of the difference of the two input frequencies will be generated. Fig. 2.4 shows the scheme of the DFG process.

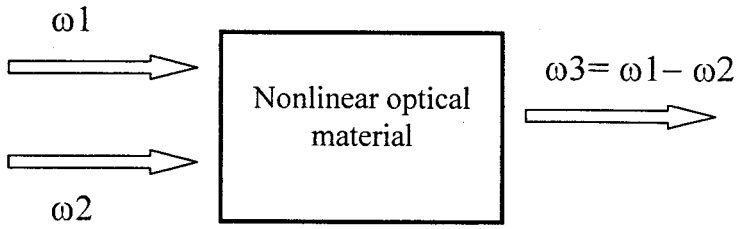

Fig. 2.4. Schematic present of DFG process

The first tunable mid-IR DFG source was realized by Pine in 1975. He mixed an argon ion laser (fixed wavelength) with a tunable CW dye laser in lithium niobate to obtain 2.2-2.4 μm tunable laser, and then he applied the laser to a high resolution spectroscopy.

Large numbers of reported papers have demonstrated mid-IR sources based on DFG [14-16]. Mid IR laser sources based on DFG have many unique advantages. First of all, it can realize continuous-wave mid IR laser at room temperature, which is impossible to semiconductor laser source. Second it can be very compact and robust source. Third, it has narrow spectral linewidth and broad and continuous tuning region. Furthermore, its tuning speed is very fast [14].

In DFG process, two near-IR laser pump sources are frequency mixed to generate mid-IR laser in nonlinear crystals, such as periodically poled $LiNbO_3$, $KTiOPO_4$ (KTP), $KTiOAsO_4$ (KTA), $AgGaS_2$, $AgGaSe_2$ [14-16].

The optical transparency range limit is about 5.5μm for $LiNbO_3$, 4.5μm for KTP, and 5.3μm for KTA. To obtain mid-IR laser in 2-6μm region, $LiIO_3$ and $LiNbO_3$ crystals are mainly used. In this spectral region the crystals have high transparency as mentioned

above, relatively high optical breakdown thresholds, and high nonlinear coefficients, while $AgGaS_2$ and $AgGaSe_2$ are most often used in the wavelength range from 4 to 23 μm [16].

In order to efficiently generate DFG, phase-matching (i.e. momentum conservation) between the three waves must be satisfied. For this purpose, either the birefringent phase-matching technique or quasi-phase-matching technique (QPM) can be used. The idea of using QPM-DFG wavelength converters was first proposed in 1962. Recently QPM DFG with very high efficiency has been demonstrated [17].

Recently, there have been several demonstrations of mid IR generation by quasi-phase-matched (QPM) in periodically poled $LiNbO_3$ (PPLN) material [14, 18]. QPM in PPLN has several unique advantages: first, PPLN has high nonlinear coefficient d_{33}, which is substantially higher than other materials; second, it can be used over a wide wavelength range from approximately 350nm to 5μm; thrid, noncritical phase-matching with zero walk-off is possible in PPLN crystal; last, lithium niobate is commercially produced in much larger quantities than other nonlinear crystal, and consequently gives high quality, reproducible crystals [14].

It turns out that the DFG based mid-IR source has several spectroscopic features, such as wide, smooth, continuous tunable CW radiation, narrow linewidth, high resolution and high sensitivity. Also, it can be operated at room temperature.

2.2.2 Optical Parametric Oscillation

Optical Parametric Generation (OPG) is an inverse process of Sum Frequency Generation. It splits one high - frequency photon (pumping wavelength) into two low -

frequency photons (signal, and idler wavelength). If two mirrors are added to form a cavity, an Optical Parametric Oscillator (OPO) is established. Fig. 2.5 shows the process of OPO. For a fixed pump wavelength, an infinite number of signal and idler wavelengths can be generated by tilting a crystal. Therefore, OPO is an excellent source for generating wide tunable range coherent radiation.

The parametric process can also be used in optical parametric amplifiers (OPA) to boost infrared output powers. CW OPOs amplified by pulsed OPAs offer a competitive alternative to other tunable lasers in the 1 – 5 μm spectral region in terms of linewidth, wavelength tunability and output powers. Also, KTP and $LiNbO_3$ are good crystals for OPO and OPA applications.

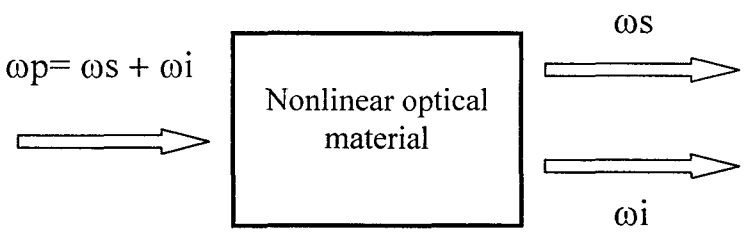

Fig. 2.5. Optical parametric oscillator (OPO) process

2.3 Conclusion of several types of laser sources

As described above, the methods to achieve mid-IR lasers have their own advantages and also drawbacks. In the past, direct semiconductor lasers and quantum cascade lasers, which are very compact, have been used for detection of trace gases for long time. However, they have some obvious disadvantages. For example, their tunable regions are

limited, which can't satisfy the needs of practical applications. Furthermore, they have to be operated at very low temperature, which means that they can't be realized at room temperature [19]. As to the OPO process, its drawback is that its spectral linewidths are large and require improvements in effective single frequency control and scanning. So they can't be used in the fields where high sensitivity and selectivity are required [10, 11].

The advantages of the DFG based sources over the existing lead salt diode lasers, antimonide diode lasers and multiple quantum well lasers, which operate in the same wavelength region, are broad tunable wavelength region, narrow linewidth, room temperature operation, low noise, low power consumption, compact size and ruggedness.

2.4 Applications of mid-IR lasers based on DFG

As discussed above, based on DFG, CW narrow-linewidth tunable mid-IR radiation sources have many useful applications, including:

- Fiber-optics chemical sensors,
- Biomedical technology,
- High-resolution spectroscopy,
- Molecular spectroscopy,
- Pollution monitoring and trace gas detection.

Among the applications, mid-IR laser used in environmental analysis and trace gas detection has attracted most attention. CW narrow-linewidth tunable mid-IR lasers near 3-5 μm region have been proved to be suitable sources for trace gas detection. Most of

the gas species have very high absorption strengths in this mid-IR region. For example, the absorption wavelength is 3.0 μm for ammonia (NH_3), 3.3 μm for methane (CH_4), 3.5 μm for formaldehyde (H_2CO), and 4.3 μm for carbon dioxide (CO_2). A significant issue in urban air quality monitoring is the ability to measure particular trace gas and pollutant gases, such as CO, N_2O, CO_2, SO_2, H_2CO, and CH_4 in real time with high sensitivity and selectivity. H_2CO is a precursor to atmospheric ozone production, although at low concentrations of 2 to 20 ppb. In major urban environment, monitoring of H_2CO distribution and its daily concentration cycle is important in modeling complex ozone chemistry. CO_2 and CH_4 have been pointed out as being responsible for the greenhouse effects, which have warmed up the atmosphere by one degree in one century. The increase of the concentration of the CO has been held responsible for a consecutive increase of the breathing troubles. As a result, there is a strong demand to detect and measure these gases quantitatively.

Since most molecules have fundamental vibration absorption lines in the infrared wavelength region from 2 μm to 5 μm (as shown in table below), laser absorption spectroscopy is considered as the most effective technique to detect the trace gases because of its high sensitivity and selectivity. Each type of the molecule has its own signature constituted of lines with well-defined positions and can hence be identified without the trace of a doubt. To develop practical trace gas detection sensors based on the laser absorption spectroscopy, affordable compact, room-temperature operation, and broadly tunable mid-IR laser sources with the following features are crucial.

- Tunable mid-IR source in the 2 to 5 μm region;
- Frequency agility: rapidly address relevant spectroscopic targets;

- Rapid, precise tuning in the region for real-time spectral profiling;
- Narrow line width ± 100MHz for resolving complex overlapping spectra;
- Sufficient power for spectroscopic measurements.

The Table below shows typical gas species accessible by mid-IR sensors and detectable concentration (assuming 10-5 absorbance, 1 Hz bandwidth and one meter path)

Table 2.5. Summary of gas absorption regions and detection limit.

Gas species	**Wavelength (nm)**	**Concentration (ppb)**
CO	4600 2330	0.75 500
N_2O	4470 2260	0.44 1000
CO_2	4230	0.13
SO_2	7280	14
H_2CO	3550	8.4
CH_4	3260	1.7
HCl	3400	0.83
HBr	3820	7.2

Significant efforts have been made worldwide to develop mid-IR laser sources for the trace gas detection. High performance laser sources satisfying the above mentioned requirements are scarce when the wavelength of interest falls in the mid-IR of 2 to 5 μm band. As described above, antimonide based semiconductor lasers and quantum cascaded lasers have been demonstrated to generate the mid-IR light. Despite the excellent compactness feature of the semiconductor lasers, unfortunately, there is presently no semiconductor laser able to be operated in CW mode beyond 2.7 μm at room temperature. From 3 to 5 μm, practically a cooling at liquid nitrogen temperature remains necessary. Much effort has been paid on fabricating the mid-infrared lasers by using Ho or Er doped YAG or fiber as a laser medium. However, the reported mid-infrared lasers can only operate at fixed wavelength, which is obviously not able to satisfy the requirement for practical trace gas detections where widely tunable lasers are desired. Other sources include LED and optical parametric oscillators. The former is an excellent compact robust source. However, the broad bandwidth feature of LED prevents its applications in high sensitive and high selective trace gas detection. The latter, while not truly a laser, is showing more and more promise as infrared materials ($AgGaSe_2$, $ZnGeP_2$) and periodically poled materials ($LiNbO_3$, KTP) develop at a frantic pace with improved conversion efficiencies. However, their spectral emission bandwidth is large, making spectroscopy impossible for those trace gas species with narrow absorption linewidths.

Recently, DFG technique has attracted much attention since it allows commercially available near-infrared, narrow linewidth laser sources to be frequency shifted into the mid-infrared region. Microwatt level radiation has been achieved with fiber amplified

single-frequency diode pump lasers using a nonlinear crystal such as periodically poled lithium niobate (PPLN). Tunable single frequency mid-infrared radiation with a tuning range of up to 450 nm and microwatt output with a sub-100MHz linewidth has been reported, based on DFG in bulk PPLN pumped by a 1083 nm diode laser seeded Yb-doped double cladding fiber amplifier and an external cavity diode laser (ECDL) tunable from 845 to 865 nm. To increase the DFG power, an architecture based on two frequency-stable diode lasers at 1.1 and 1.5 μm, which is amplified by high power Yb and Er/Yb fiber amplifiers has been proposed. 0.7 mW of narrow-band (<60 MHz) mid-IR light with limited tunable range has been achieved.

Although DFG based mid-IR sources have advantages such as room temperature operation, intrinsic wavelength stability, and high beam quality, their low CW power (~μW in most cases) has limited their minimum detection sensitivities. For multi-species detection, tunable range of the DFG based mid-IR source has to be further enhanced to cover the whole band of 2 to 5 μm with a single crystal.

References for chapter 2

[1]. Nilesh J. Vasa, Husayin Parhat, Masahiro Kidosaki, Tatsuo Okada, Mitsuo Maeda, Hirokazu Taniguchi, Masaru Nakamura, CLEO Pacific Rim 99, pp. 181-182(1999).

[2]. Frank K. Tittel, Dirk Richter, and Alan Fried, "Mid-Infrared Laser Applications in Spectroscopy", 2002

[3]. Goyal A.K., Sanchez A, Turner G.W., Fan T.Y., Liau Z.L., Manfra M.J., Foti P.J., Missaggia L., O'Brien P., Daneu J.L., Lasers and Electro-Optics Society **2**, 532-533(2001).

[4]. P. F. Moulton: Tunable solid-state lasers, Proc. IEEE **80**, 348 - 364 (1992)

[5]. N.P. Barnes, F. Allario, Proc. SPIE **868**, 107 - 116 (1988)

[6]. S. K ¨ uck, Applied Physics B-Lasers & Optics B **72**, 515 - 562 (2001)

[7]. Mariano Troccoli, Federico Capasso, CLEO Technical Digest **1**, 15-19(2003).

[8]. F. Capasso, C. Gmachl, R. Paiella, A. Tredicucci, A.L. Hutchinson, D.L. Sivco, J.N.Baillargeon, A.Y.Cho, H.C.Liu, IEEE Quant.Electron.6. 931-947 (2000)451,489

[9]. C.Gmachl, A.Straub, R.Colombelli, F.Capasso, D.L.Sivco, A.M.Sergent, A.Y.Cho, IEEE Quantum Electron. **38. 569 .581**, 451 (2002)

[10]. M. Feher, P. a. Martin, Spectrochim. Acta Pt. A **52**, 1579(1995).

[11]. Phillips, P.J., Das, S., Ebrahimzadeh, M., Lasers and Electro-Optics, Conference on

7-12 May 2000, pp. 155 - 156 .

[12]. Bohren, A., Sigrist, M.W., lasers and Electro-Optics, 1999. CLEO. Summaries of Papers Presented at the Conference on 23-28 May 1999, pp. 190 – 191

[13]. L. E. Myers, J. Opt. Soc. Amer. B **12**, 2102-2106(1995).

[14]. Nilesh J. Vasa, Husayin Parhat, Masahiro Kidosaki, Tatsuo Okada, Mitsuo Maeda, Hirokazu Taniguchi, Masaru Nakamura, CLEO Pacific Rim 99, pp. 181-182(1999).

[15]. K.Fradkin-Kashi, A. Arie, P. Urenski, G.. Rosenman, Opt. Lett. **25**, 743-745 (2000).

[16]. T. Kaing, D. Lee, J.-J. Zondy, IEEE Conference on 6-10 July, 1998, pp. 157-158.

[17]. M. H. Chou, I. Brener, G. Lenz, R.Xcptto, E.E. Chanban, J. Shmulovich, S. Philen, S. Kosinski, K.R.Parameswaran, M.M.Fejer, IEEE Photonics Technol. Lett. **12**, 82-84(2000)

[18]. L. Goldberg, W.K.Burns, R.W.McElhanon, Opt. Lett. 20, 1280-1282(1995).

[19]. D. Richter, A. Fried, B. P. Wert, J. G.. Walega, F.K.Tittel, Appl. Phys. B **75**, 281-288(2002).

CHAPTER 3:

DIFFERENCE–FREQUENCY GENERATION AND CHARACTERISTICS OF LITHIUM NIOBATE

3.1 Nonlinear optical process

In linear optics, usually, the polarization is assumed to be linearly related with the input light electric field. In case of a linear medium, the electric displacement can be written with the electric field and permittivity as follows

$$\mathbf{D} = \varepsilon \mathbf{E} = \varepsilon_0 \mathbf{E} + \mathbf{P}_L \tag{3.1}$$

Electrical displacement consists of the vacuum contribution $\varepsilon_0\mathbf{E}$ and the induced polarization in an optical medium $\mathbf{P}_L$. This linear polarization can also be written using susceptibility.

$$\mathbf{P}_L = \varepsilon_0 \chi^{(1)} \mathbf{E} \tag{3.2}$$

The linear susceptibility can be written as follows:

$$\chi^{(1)} = \frac{\varepsilon}{\varepsilon_0} - 1 \tag{3.3}$$

In some materials higher order processes can be observed at large field amplitudes. Next, we will discuss the nonlinear case. In nonlinear optics, the optical response can often be described by expressing the polarization $\mathbf{P}(t)$ as a power series

in the field strength **E**(t) as follows [1]:

$$\begin{aligned}\mathbf{P}(t) &= \varepsilon_0\chi^{(1)}\mathbf{E}(t) + \varepsilon_0\chi^{(2)}\mathbf{E}^2(t) + \varepsilon_0\chi^{(3)}\mathbf{E}^3(t) + \ldots \\ &= \mathbf{P}^{(1)}(t) + \mathbf{P}^{(2)}(t) + \mathbf{P}^{(3)}(t) + \ldots\end{aligned} \tag{3.4}$$

The first term in the above equation is the linear polarization as described above. The second-order term in the above equation:

$$\mathbf{P}^{(2)}(t) = \varepsilon_0\chi^{(2)}\mathbf{E}^2(t) \tag{3.5}$$

is called second-order nonlinear polarization.

Now, considering two light fields with two different frequencies impinging on the crystal [1]:

$$E = E_1 e^{i\omega 1 t} + E_2 e^{i\omega 2 t} \tag{3.6a}$$

To simplify, just consider the real part of the Electric field:

$$E = E_1\cos(\omega_1 t) + E_2\cos(\omega_2 t) \tag{3.6b}$$

The second order term then becomes:

$$\begin{aligned}P_2 &= \varepsilon_0\chi^{(2)}[E_1^2\cos^2(\omega_1 t) + E_2^2\cos^2(\omega_2 t) + E_1E_2\cos(\omega_1 t)\cos(\omega_2 t)] \\ &= \varepsilon_0\chi^{(2)}\left[\frac{1}{2}(E_1^2 + E_2^2) + \frac{1}{2}E_1^2\cos(2\omega_1 t) + \frac{1}{2}E_2^2\cos(2\omega_2 t)\right] \\ &\quad + \varepsilon_0\chi^{(2)}\left[E_1E_2\cos[(\omega_1 + \omega_2)t] + E_1E_2\cos[(\omega_1 - \omega_2)t]\right]\end{aligned} \tag{3.7}$$

The output consist of a time independent dc term, a second harmonic term, $2\omega_1$ and $2\omega_2$, and two terms involving new frequencies:

$\omega_1 + \omega_2$: Sum Frequency Generation (SFG)

$\omega_1 - \omega_2$: Difference Frequency Generation (DFG)

Fig. 3.1 (a) Scheme of SFG process (b) Scheme of DFG process

Then, we can describe the difference-frequency generation in photon energy-level description.

When two photons at frequencies ω_1 and ω_3 (assuming $\omega_3 > \omega_1$) are incident on a crystal with an appreciable second-order susceptibility $\chi^{(2)}$ (as shown in figure 10. part b), a photon at frequency ω_2 ($\omega_2 = \omega_3 - \omega_1$) will be generated. The process of difference-frequency generation is described by a nonlinear polarization of the form:

$$P(\omega_2 = \omega_3 - \omega_1) = 2\chi^{(2)} E_1 E_2^* \tag{3.8}$$

In order to satisfy energy conservation, for every photon generated at the difference frequency ω_2, a photon at ω_1 must also be created, while a photon at the higher input frequency ω_3 must be annihilated (Fig. 3.2).[1]

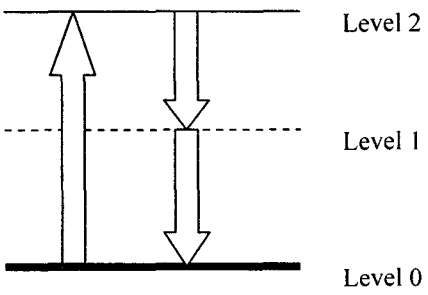

Fig. 3.2 photon energy-level description of DFG

3.2 The wave equation in nonlinear media

In a nonlinear media, the different frequency components can be coupled by a nonlinear interaction.

The appearance of the new generated frequency components can be examined using Maxwell Equations and the wave equation in the nonlinear media.

Maxwell Equations in the general form are:

$$\nabla \cdot \mathbf{D} = \rho \tag{3.9}$$

$$\nabla \cdot \mathbf{B} = 0 \tag{3.10}$$

$$\nabla \times \mathbf{E} = -\frac{\partial \mathbf{B}}{\partial t} \tag{3.11}$$

$$\nabla \times \mathbf{H} = \mathbf{J} + \frac{\partial \mathbf{D}}{\partial t} \tag{3.12}$$

In any optical medium, we can describe the relations of the input light and the materials with material equations:

$$\mathbf{J} = \sigma \mathbf{E} \tag{3.13}$$

$$\mathbf{B} = \mu \mathbf{H} \tag{3.14}$$

The polarization vector depends upon the electric field by:

$$\mathbf{D} = \varepsilon \mathbf{E} + \mathbf{P}_{\mathrm{NL}} = \varepsilon_0 \mathbf{E} + \mathbf{P}_{\mathrm{L}} + \mathbf{P}_{\mathrm{NL}} = \varepsilon_0 \mathbf{E}(1 + \chi) + \mathbf{P}_{\mathrm{NL}} \tag{3.15}$$

Here, σ is the conductivity, ε is the permittivity or dielectric constant and μ is the permeability.

$$\varepsilon = \varepsilon_0 \varepsilon_r \tag{3.17}$$

$$\mu = \mu_0 \mu_r \tag{3.18}$$

Here, ε_0 and μ_0 are permittivity and permeability in the vacuum, respectively, while ε_r and μ_r are relative permittivity and permeability, respectively.

From Maxwell Equations we can directly derive the wave equation in a medium in the case of no free charges ($\rho = 0$) by taking the curl of Faraday's equation (3.11):

$$\nabla \times \nabla \times \mathbf{E} = -\frac{\partial}{\partial t} \nabla \times \mathbf{B} \tag{3.19}$$

Using the equation (3.12) and material equations (3.13) (3.14) given above, we get the following:

$$\nabla \times \nabla \times \mathbf{E} = -\mu \frac{\partial^2}{\partial t^2} \mathbf{D} - \sigma\mu \frac{\partial}{\partial t} \mathbf{E} \tag{3.20}$$

Using equation (3.15) and $\nabla \times \nabla \times \mathbf{E} = \nabla(\nabla \cdot \mathbf{E}) - \nabla^2 \mathbf{E}$ in the case of no sources $\nabla \cdot \mathbf{E} = 0$:

$$\nabla^2 \mathbf{E} - \mu\varepsilon_0 \frac{\partial^2}{\partial t^2} \mathbf{E} - \mu\sigma \frac{\partial}{\partial t} \mathbf{E} = \mu \frac{\partial^2}{\partial t^2} \mathbf{P}_{NL} \tag{3.21}$$

Usually, in dielectric media, typically, $\sigma = 0$ and $\mu = \mu_0$ (permeability in the vacuum).

$$\nabla^2 \mathbf{E} - \mu_0\varepsilon_0 \frac{\partial^2}{\partial t^2} \mathbf{E} = \mu_0 \frac{\partial^2}{\partial t^2} \mathbf{P}_{NL} \tag{3.22}$$

Consider the three waves $\mathbf{E}_1(k_1, \omega_1)$, $\mathbf{E}_2(k_2, \omega_2)$ and $\mathbf{E}_3(k_3, \omega_3)$ interacting in a medium by second-order nonlinear polarization ($\omega_2 = \omega_3 - \omega_1$).

For DFG with high conversion efficiency, the following conditions usually exist: the coupled waves are collinearly phase matched, the medium is nearly lossless, and the slowly varying amplitude approximation is valid.

Then coupled Equations can be derived as follows [1]:

$$\frac{\partial \mathbf{E}_1(z)}{\partial z} = -\frac{i2\pi\omega_1^2}{k_1 c^2} \chi^{(2)}(\omega_1) : \mathbf{E}_2^*(z)\mathbf{E}_3(z)e^{-i\Delta kz} \tag{3.23}$$

$$\frac{\partial \mathbf{E}_2(z)}{\partial z} = -\frac{i2\pi\omega_2^2}{k_2 c^2}\chi^{(2)}(\omega_2):\mathbf{E}_3(z)\mathbf{E}_1^*(z)e^{-i\Delta kz} \tag{3.24}$$

$$\frac{\partial \mathbf{E}_3(z)}{\partial z} = -\frac{i2\pi\omega_3^2}{k_3 c^2}\chi^{(2)}(\omega_3):\mathbf{E}_1(z)\mathbf{E}_2(z)e^{i\Delta kz} \tag{3.25}$$

In the infinite plane wave approximation, when assuming E_3 is constant, the output solution is:

$$E_2 = \frac{\omega_2^2 z}{k_2} K E_3 E_1^* \frac{\sin(\Delta kL/2)}{\Delta kL/2} \tag{3.26}$$

$$I_2 = \frac{8\pi^3\omega_2^2}{c^3 n_1 n_2 n_3}\chi^{(2)}(\omega_2)z^2\frac{\sin^2(\Delta kL/2)}{(\Delta kL/2)^2}I_3 I_1 \tag{3.27}$$

Here, n1, n2, n3 are the refractive indices of the lights of frequency $\omega_1, \omega_2, \omega_3$ in the media. $\chi^{(2)}(\omega_2)$ is the second order susceptibility of the difference frequency light. I_1 and I_3 are the intensities of the signal and pump light. Δk is the so-called phase mismatch: $\Delta k = 2\pi(\frac{n_1}{\lambda_1}+\frac{n_2}{\lambda_2}-\frac{n_3}{\lambda_3})$.

The plane wave approximation adopted here is good as long as the output wavelength is much smaller than the beam cross section. The results describe mid-IR generation by difference frequency mixing very well.

3.3 PPLN and Quasi-phase matching

In equation 3.27, it can be seen that the intensity of the difference frequency wave oscillates between zero and its maximum value along the propagation direction. The

major factor affecting the intensity is the phase difference Δk. When $\Delta k = 0$, the output intensity increase quadratically along the propagating axis. The condition $\Delta k = 0$ is the so-called phase-matching condition. The generated intensity depends strongly on the phase-matching condition. The phase matching condition should be satisfied, if efficient DFG needs to be achieved.

Typically, three-wave mixing is done in a birefringent crystalline material (I.e., the refractive index depends on the polarization and direction of the light that passes through.), where the polarizations of the fields and the orientation of the crystal are chosen such that the phase-matching condition is fulfilled. This phase matching technique is called angle tuning. Typically a crystal has three axes, one of which has a different refractive index than the other ones. This axis is called the extraordinary (e) axis, while the other two are ordinary axes (o). There are several schemes of choosing the polarizations. If the signal and idler have the same polarization, it is called "Type-I phase-matching", and if their polarizations are perpendicular, it is called "Type-II phase-matching". However, other conventions exist that specify further which frequency has what polarization relative to the crystal axis. These types are listed below, with the convention that the signal wavelength is shorter than the idler wavelength.

Table. 3.1 Comparison of different types of phase-matching ($\lambda_p \leq \lambda_s \leq \lambda_i$)

Phase-matching types Polarizations			**Scheme**
Pump	**Signal**	**Idler**	
e	o	o	Type I
e	o	e	Type II (or IIA)
e	e	o	Type III (or IIB)
e	e	e	Type IV
o	o	o	Type V
o	o	e	Type VI (or IIB or IIIA)
o	e	o	Type VII (or IIA or IIIB)
o	e	e	Type VIII (or I)

Most common nonlinear crystals are negative unaxial, which means that the *e* axis has a smaller refractive index than the *o* axes. In those crystals, type I and II phasematching are usually the most suitable schemes. In positive uniaxial crystals, types VII and VIII are more suitable. Types II and III are essentially equivalent, except that the names of signal and idler are swapped when the signal has a longer wavelength than the idler. For this reason, they are sometimes called IIA and IIB. The

type numbers V–VIII are less common than I and II and variants.

One undesirable effect of angle tuning is that the optical frequencies involved do not propagate collinearly with each other. This is due to the fact that the extraordinary wave propagating through a birefringent crystal possesses a Poynting vector that is not parallel with the propagation vector. This would lead to beam walkoff which limits the nonlinear optical conversion efficiency. Two other methods of phase matching avoid beam walk-off by forcing all frequencies to propagate at a 90 degree angle with respect to the optical axis of the crystal. These methods are called temperature tuning and quasi-phase-matching.

Temperature tuning is where the pump (laser) frequency polarization is orthogonal to the signal and idler frequency polarization. The birefringence in some crystals, in particular Lithium Niobate is highly temperature dependent. The crystal is controlled at a certain temperature to achieve phase matching conditions.

The other method is quasi-phase matching. Historically, the technique of quasi-phase matching was first proposed by Armstrong etal. [2]. But there were still limits in optical materials and birefringent crystals were the only choices for phase matching until mid 1990's.

Quasi-phase-matching does not depend on birefringence, but instead, on a periodic sign reversal every coherence length of the nonlinear coefficient in the optical materials. So far, permanent sign reversal is most efficiently achieved with electric field poling in ferro-electric materials such as $LiNbO_3$ [3], $LiTaO_3$ [4], $KTiOPO_4$ [5], and $RbTiOAsO_4$ [6].

In this method the frequencies involved are not constantly locked in phase with each other, instead the crystal axis is flipped at a regular interval Λ. Hence, these crystals are called periodically-poled. This results in the polarization response of the crystal to be shifted back in phase with the pump beam by reversing the nonlinear susceptibility. This allows net positive energy flow from the pump into the signal and idler frequencies. In this case, the crystal itself provides the additional wave vector $k=2\pi/\lambda$ (and hence momentum) to satisfy the phase matching condition. Quasi-phase-matching can be expanded to chirped gratings to get more bandwidth and to shape a SHG pulse like it is done in a dazzler. Table 3.2 gives the comparison of quasi-phase-matching and birefringent phase-matching. It can be concluded from Table 3.2 that quasi-phase matching has several advantages, especially it can achieve phase-matching of any wavelength combinations.

Table 3.2. Comparison of Quasi phase-matching and birefringent phase-matching [7]

Quasi - Phase Matching	**Birefringent Phase Matching**
• Noncritical phase matching (no walkoff)	• Mostly critical phase matching (walkoff)
• Larger diagonal nonlinear coefficients can be used	• Only smaller, non-diagonal coefficients can be used
• Phase match any wavelength combinations within crystal transparency	• Limited phase matching (e.g. no blue SHG for $LiNbO_3$)
• Tuning via temperature, multiple or continuous fan-out type grating periods	• Tuning via temperature and angle
• Wide acceptance bandwidth / angle, easy to align	• Limited acceptance bandwidth / angle, difficult to align
• User design friendly criteria	

In QPM, the sign of the nonlinear coefficient is reversed every coherence length, causing the locally generated polarization field to transfer power to the harmonic beam. By compensating for phase-velocity mismatch in this way, the largest elements of a crystal's nonlinear tensor can be accessed throughout the entire transparency range. Figure 3.3 shows the effect of QPM on I (ω_2) over the length of propagation in SHG process. In the non-phase matched case, the generated I (ω_2) grows and reaches a maximum at z = lc. With further propagation E (ω_2) begins to shrink returning to zero at z = 2 lc. In the QPM case, the sign of the nonlinear interaction is reversed every lc. This is achieved by reversing the sign of d (z). The resultant I (ωi) grows monotonically.

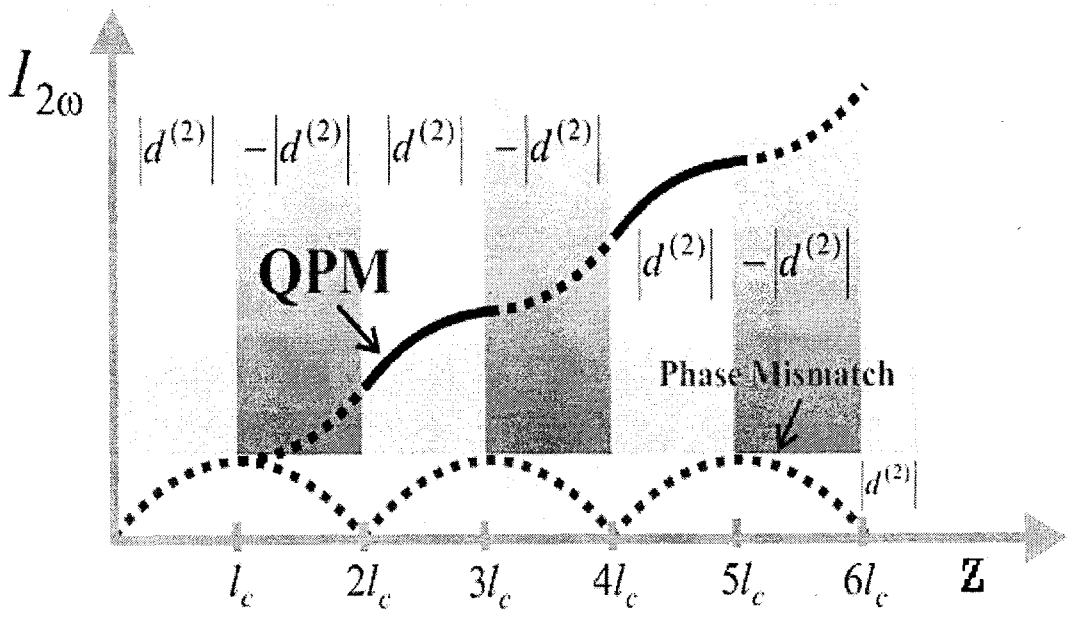

Fig. 3.3 QPM effect on I (ωi) [8].

The equation governing QPM for DFG is the following:

$$\frac{n_p}{\lambda_p} - \frac{n_s}{\lambda_s} - \frac{n_i}{\lambda_i} - \frac{1}{\Lambda} = 0$$

where n_p, n_s, n_i are the refractive indices of pump, signal and idler lasers, respectively. And Λ is the inverse period of the nonlinear materials. Therefore, the appropriate grating period can be calculated from the above equations.

In practice, it is difficult to make a perfect QPM grating in a nonlinear crystal. Factors such as uncertainty in exact value of material constants, fabrication errors, and the change of material constants due to the fabrication process may give rise to a residual phase mismatch.

3.4 Characteristics of Lithium Niobate

3.4.1 Nonlinear properties of lithium niobate crystal

In frequency conversion processes discussed above, appropriate nonlinear optical crystals are required. So far, many nonlinear optical crystals have been developed for the use of nonlinear frequency conversion. For example, Lithium Niobate ($LiNbO_3$), Lithium Tantalate ($LiTaO_3$), Potassium Titanium Oxide Phosphate ($KTiOPO_4$ / KTP), Lithium Triborate (LiB_3O_5 / LBO), Potassium Dihydrogen Phosphate (KDP), and Beta Barium Borate (Beta-BaB_2O_4 / BBO) have all been successfully used.

Among these nonlinear optical crystals, $LiNbO_3$, which is described as "the silicon of nonlinear optics", has been successfully used in various nonlinear optical

processes and is an excellent choice for many applications. This is because it has many special characteristics, which will be discussed later in this chapter. Single crystals of this material were first prepared by using the Czochralski technique of pulling from the melt by Ballman (1965) [9].

Table 3.3 summarizes some properties of $LiNbO_3$ and some of other mid-IR nonlinear crystals, including GaSe, $AgGaSe_2$, $AgGaS_2$.

Table 3.3 The properties of $LiNbO_3$ compared with some of other mid-IR nonlinear crystals [10]

Properties	**GaSe**	**$AgGaSe_2$**	**$AgGaS_2$**	**$LiNbO_3$**
Uniaxial crystal	negative($n_o>n_e$)	negative($n_o>n_e$)	negative($n_o>n_e$)	negative($n_o>n_e$)
Point group	62m	42m	42m	3m
Transparency range (μm)	0.65-18	0.71-18	0.5-13	0.33-5.5
Typical values of index (@10.6 μm)	n_o=2.8136 n_e=2.4389	n_o=2.5915 n_e=2.5585	n_o=2.3466 n_e=2.2924	n_o=2.2340 n_e=2.1554 (@1.06 μm)
Effective nonlinearity d_{eoo} d_{eoe}	$d_{22}\cos\theta\sin3\varphi$ $d_{22}\cos^2\theta\cos3\varphi$	$d_{36}\sin\theta\sin2\varphi$ $d_{36}\sin2\theta\cos2\varphi$	$d_{36}\sin\theta\sin2\varphi$ $d_{36}\sin2\theta\cos2\varphi$	$d_{15}\sin\theta - d_{22}\cos\theta\sin3\varphi$ $d_{22}\cos^2\theta\cos3\varphi$
Nonlinear coefficient (10^{-11} m/V, @10.6μm)	d_{22}=5.44±0.1	d_{36}=3.3±0.3	d_{36}=1.34±0.25	d_{15}(1.06μm)=-0.544 d_{22}(1.06μm)=0.276
Nonlinear figure of merit($\frac{d^2}{n^3}$) (10^{-24} m^2/V^2, @10.6 μm)	152	63	14	
Surface-damage threshold ($10^6 Wcm^{-2}$, @1.06 μm)	35 (τ_p=10ns)	30 (τ_p=35ns)	25 (τ_p=35ns)	120 (τ_p=30ns)
Linear absorption(cm^{-1}) (@1.9 μm)	0.1	0.089	<0.09	0.08

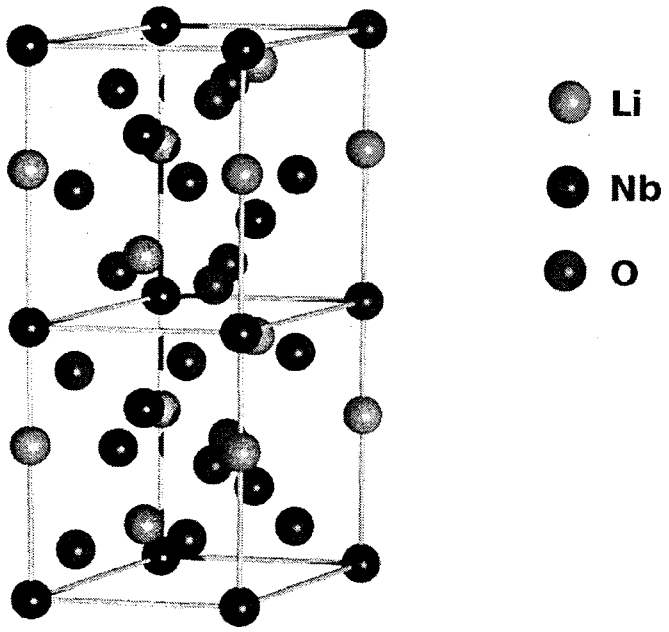

Fig, 3.4. Fundamental hexagonal crystal structure of $LiNbO_3$

$LiNbO_3$ is a compound of niobium, lithium, and oxygen. It is a colorless solid material with trigonal crystal structure. Fig. 3.4 shows the fundamental hexagonal crystal structure of $LiNbO_3$. It is transparent for wavelengths between 350 and 5200 nm and has a bandgap of around 4 eV. Its melting point is 1257 ^{o}C and its density is 4.65 g/cm^3. It is insoluble in water. And its CAS number is [12031-63-9] [11].

Fig. 3.5 shows that $LiNbO_3$ crystals have trigonal (three-fold rotation) symmetry in the high temperature phase [11]. The oxygen planes are represented by lines, and the cations are centered on, or between the planes. The cations are displaced from the center position, defining the direction of the polar C-axis.

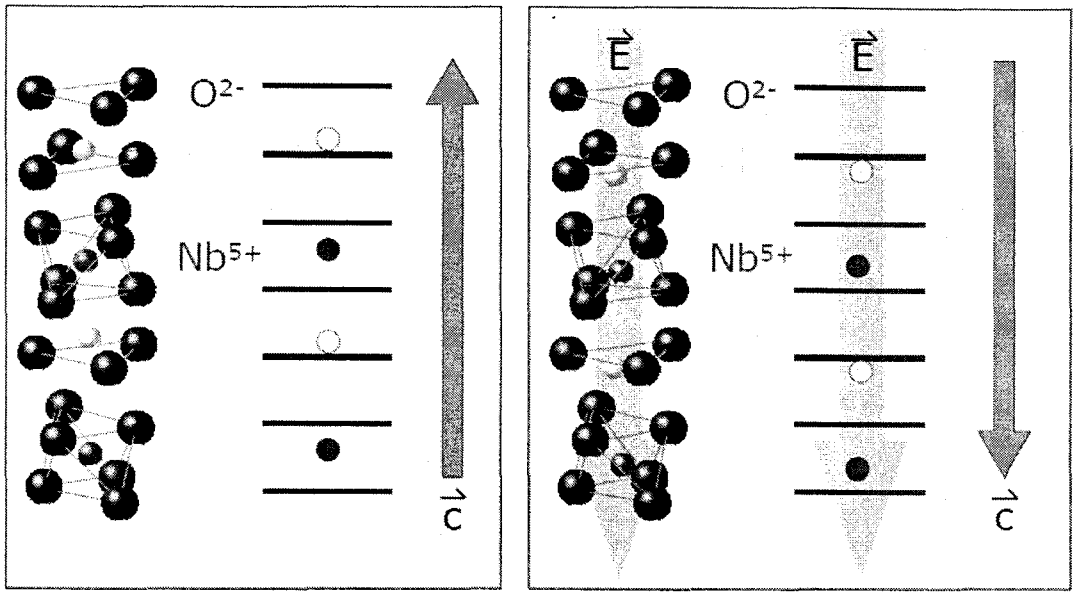

(a) (b)

Fig. 3.5 (a) The ferroelectric polarization of lithium niobate. (b) The para-electric polarization of lithium niobate. [12]

In $LiNbO_3$ crystals, the electronic charge shifts more easily, when the electric field is applied in a specific direction. When it is cooled, the spontaneous polarization aligns with symmetry axis, so only two directions are possible. Therefore, no further phase transition is observed below the phase transition temperature, which is called Curie temperature, and there is no structural mismatch between neighboring domains. A displacement of the cations between the oxygen lattices causes the transition as shown in Fig. 3.5. This allows the production of large crystals without the risk of fracturing at the phase transition temperature. To be useful, the uniformly poled crystals are desired where the whole crystal has a spontaneous polarization pointing in the same direction. This can be achieved by a poling step after growth. An electric field is applied while the crystal is cooled through the phase transition temperature

(Curie temperature). At that temperature, the developing spontaneous polarization will align itself along the polarization with respect to the applied electric field, and we can achieve a single-domain crystal. Within each domain, all the cations are displaced in one direction, adding to a spontaneous polarization at no applied field in that direction. This property makes $LiNbO_3$ an appropriate material for the fabrication of domain inversion gratings.

Furthermore, $LiNbO_3$ is chosen as a main material in various applications because of the following reasons.

First, the market volume of $LiNbO_3$ is large, which is about 150 tons per year and about 40 million dollars' sales per year. Its production is mainly in China, US and Japan using a very stable fabrication technology.

Second, as mentioned above, $LiNbO_3$ is transparent for wavelengths between 350 and 5200 nm and has a bandgap of around 4 eV, providing low loss for all the fundamental, UV, visible and mid-infrared light generation.

Last but not least, $LiNbO_3$ has the highest figure of merit (~73 pm^2/V^2 at 1064 nm) of all traditionally used nonlinear-optic crystals.

Most importantly, the QPM technique in the $LiNbO_3$ crystals has reached a mature and commercial stage [13].

$LiNbO_3$ can be used extensively in the telecoms market, such as mobile telephones and optical modulators. It is also the material of choice for the manufacture of surface acoustic wave devices. The $LiNbO_3$ crystals lack inversion symmetry and display Pockels effect. The birefringence of lithium niobate is highly

temperature dependent; accurate heating of the crystal can be therefore used to achieve phase matching in the medium. Czochralski-grown monocrystals have unique electro-optical, piezoelectric, photoelastic and nonlinear optical properties. They are strongly birefringent. They are used in laser frequency doubling, nonlinear optics, Pockels cells, optical parametric oscillators, Q-switching devices for lasers, other acousto-optic devices, optical switches for gigahertz frequencies, etc. It is an excellent material for manufacture of optical waveguides.

$LiNbO_3$ crystal can be doped by magnesium oxide (MgO) [14], which will increase its resistance to optical damage or photorefractive damage. Other available dopants are Fe, Zn, Hf, Cu, Gd, Er, Y, Mn and B, creating optical sources that can be modulated by traveling-wave waveguide modulators.

4.2 Dispersion equation of lithium niobate

Sellmeier equation for the extraordinary index of congruent $LiNbO_3$ was derived by Jundt [15], which can be applied to wavelengths from as short as 0.4 μm to as long as 5 μm. The equation is given by

$$n_e^2 = a_1 + b_1 f + \frac{a_2 + b_2 f}{\lambda^2 - (a_3 + b_3 f)^2} + \frac{a_4 + b_4 f}{\lambda^2 - a_5^2} - a_6 \lambda^2 \tag{4.1}$$

$$\begin{aligned} f &= (T - T_0)(T + T_o + 2 \times 273.16) \\ &= (T - 24.5^o C)(T + 570.82) \end{aligned} \tag{4.2}$$

where, n_e is the extraordinary refractive index in $LiNbO_3$, λ is the wavelength of the generated light, and T is the operating temperature. The fitting parameters included in the equation are all given in Table 3.4.

Table 3.4. Parameters used in improved Sellmier equation [15]

Parameter	Value
a_1	5.35583
a_2	0.100473
a_3	0.20692
a_4	100
a_5	11.34927
a_6	1.5334×10^{-2}
b_1	4.629×10^{-7}
b_2	3.862×10^{-8}
b_3	-0.89×10^{-8}
b_4	2.657×10^{-5}

Based on this dispersion equation of $LiNbO_3$, in DFG process, when the two input wavelengths (i.e. pump and signal) are known we can calculate the QPM period as a function of temperature by using the equations of QPM conditions. It is worth mentioning that the equation is valid up to a temperature as high as 500 °C [15].

4.3 Periodically poled lithium niobate for quasi-phase matching

Quasi-phase-matching (QPM) is a technique where an extra grating vector *Kg* is artificially introduced into the material, allowing for the compensation of an arbitrary value of phase mismatch, so that a given material can be engineered to perform a variety of mixing functions. The most common method to induce this extra vector is to introduce a periodic inversion of the sign of the second-order nonlinear coefficient. This technique has several advantages: first, a large bulk of crystal can be easily manufactured; second, the highest nonlinear coefficient of the crystal can be used, and, the conversion efficiency can be significantly improved.

Periodically poled lithium niobate (PPLN) is a periodic domain-engineered lithium niobate crystal with periodic domain inversion structure, so-called periodic poling which is shown in Fig. 3.6.

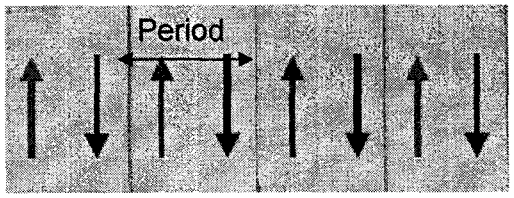

Fig. 3.6. Periodic domain inversion structure of PPLN

In recent decades, there are several groups doing research about QPM in the PPLN crystals [16 - 20]

Among the methods to fabricate PPLN, the most attractive way is the

electric-field poling technique [21].

When an electric field higher than characteristic coercive field is applied to a $LiNbO_3$ crystal, the orientation of the spontaneous polarization is reversed, which causes the reversal of the sign of the odd-rank tensor properties (such as electro-optic, piezoelectric, and nonlinear optical coefficients).

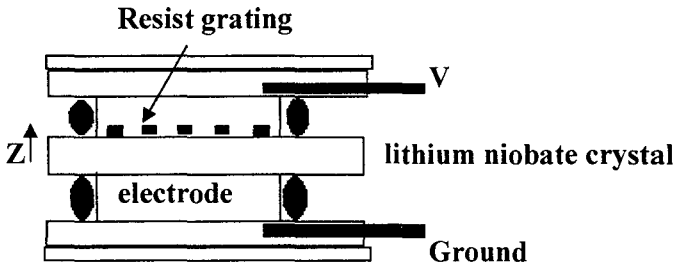

Fig. 3.7. Scheme of domain inverted fabrication by electric-field poling technique

Figure 3.7 illustrates the scheme of electric-field poling technique, where the periodic grating is achieved by applying a set of electrodes on the wafer surface before the application of high voltage. Then the not-to-patterned area is protected by a dielectric from the high voltage. The $-z$ face is mounted to the ground state, while the $+z$ face is applied with high voltage.

Typically, the voltage is around 21 kV. The assembly is suitable for producing large-area domain-inverted gratings; gratings are fabricated in full wafers without the need for a vacuum or an insulator liquid. Usually, a short-period domain inverted grating is fabricated by metal electrodes. A corona discharge method is used to fabricate the QPM grating in MgO doped $LiNbO_3$ substrates. In order to obtain highly

efficient conversion, the QPM grating must be uniform both in the depth and along the waveguide direction and the ratio between the inverted and non-inverted region in one period should be 1:1.

Other materials used for periodic poling are wide band gap inorganic crystals like KTP (resulting in periodically poled KTP, PPKTP), lithium tantalate, and some organic materials.

References for chapter 3

[1]. R. W. Boyd, "Nonlinear Optics", 2nd edition, Academic Press, Jan. 2003.

[2]. J.A. Armstrong, N. Bloembergen, J. Ducuing, and P.S. Pershan, Phys.Rev. 127, 1918-1939 (1962)

[3]. W.K. Burns, W. McElhanon, and L. Goldberg, IEEE Photon, Technol, Lett. 6, 252-254 (1994)

[4]. S.N. Zhu, Y.Y. Zhu, Z.Y. Zhang, H. Shu, H. F. Wang, J. F. Hong, C. Z. Ge, and N. B. Ming, J. Appl. Phys., 77, 5481-5483, 1995

[5]. Q. Chen and W.P. Risk, electron, Lett. 30, 1516-1517, 1994

[6]. H. Karlsson, F. Laurell, P. Henriksson, G. Arvidsson, Electron. Lett. 32, 556-557 (1996)

[7]. Michael L. Bortz, "Quasi-Phasematched Optical Frequency Conversion in Lithium Niobate Waveguides", Edward L. Ginzton Laboratory, Stanford University, Dec. 1994

[8]. A. Yariv, "Optical Electronics in Modern Communications," Oxford University Press, New York (1997).

[9] T. Matthias, and J. P. Remeika, Phys. Rev. **76** (12), 1886-1887, 1949.

[10]. Martin J. Webber, "Handbook of Laser Science and Technology, Volume III Optical Materials: Part 1", CRC Press, 1988

[11] http://en.wikipedia.org/wiki/Lithium_niobate

[12] A. Räuber, Current topics in materials science 1, ed. E. Kaldis(Amsterdam:

North-Holland), pp. 481-601, 1978.

[13] S. Wang, V. Pasiskevcius, J. Hellstrom, and F. Laurell, Opt. Lett. **24** (14), 978-980, 1999.

[14] A. Harada and Y. Nihei, Applied Physics Letters **69** (18), 2629-31 (1996).

[15] Dieter H, Jundt, Opt. Lett. **22**, 1553-1555 (1997).

[16] [M. Yamada, N. Nada, M. Saitoh, and K. Watanabe, Appl. Phys. Lett. **62**(5), 435-436, 1993.

[17] S. Matsumoto, E. J. Lim, H. M. Hertz, and M. M. Fejer, Electron. Lett. **27** (22), 2040-2042, 1991.

[18] G. A. Magel, M. M. Fejer, and R. L. Byer, Appl. Phys. Lett. **56** (2), 108-110, 1990.

[19] H. Ito, C. Takyu, and H. Inaba, Electron. Lett. **27** (14), 1221-1222, 1991.

[20] S. Miyazawa, J. Appl. Phys. **50** (7), 4599-4603, 1979.

[21] C.Q. Xu, invited, Proc. of The 4th Asia Pacific International Symposium on the Basic and Application of Plasma Technology, 2005, Taiwan, R.O.C., pp. 49-53

CHAPTER 4:
EXPERIMENTAL RESULTS OF PPLN BASED DFG TUNABLE MID-IR LASER SOURCES

4.1 Experimental arrangement of QPM DFG in bulk PPLN

In this chapter, a mid-IR laser source based on DFG in a PPLN crystal with certain periods is demonstrated, and the wavelength tuning characteristics of mid-IR light generation in PPLN crystals are experimentally studied. Widely tunable coherent mid-IR radiation from 3.7 μm to 4.7 μm was produced by mixing a cw Nd:YAG laser at 1.064 μm with a Ti:Sapphire laser tunable from 770 nm to 780 nm in a PPLN crystal with a period of 22.7 μm.

The experimental setup of DFG is schematically shown in Fig. 4.1. The signal laser was a 1-W (maximal output power) diode-pumped monolithic cw Nd:YAG laser (InnoLight, mod. Mephisto 1000) at 1.064 μm. The pump laser was a 1-W (maximal output power) tunable Ti:Sapphire laser (Coherent, Inc) with line-width of 500 kHz, which had the tunable range from 780 nm to 880 nm. The Ti:Sapphire laser was pumped by a Verdi-10 laser (Coherent). The beams of the two lasers were combined by a dichroic mirror. And the combined beam of pump laser and signal laser was directed and focused onto the center of the PPLN crystal using a K9 lens with a focus length f = 250 mm. The beam of the Ti:Sapphire laser was modulated by a mechanical chopper with a chopping frequency around 1200 Hz, allowing for the signal to be

detected with a lock-in amplifier (EG&G Model 5302). The wavelength of the Nd:YAG laser was fixed at 1.064 μm, while the Ti: Sappire laser wavelength was tuned between 780 nm and 880 nm. Continuous frequency scan of the idler laser was performed by the continuous tuning of the Ti:Sapphire laser frequency. The samples were mounted on a temperature-controlled holder, which is designed to offer optimum temperature control of the PPLN crystal. The temperature stability of the temperature controller is better than ± 0.1 °C. After wavelength mixing and conversion in the PPLN crystal, the output laser beams, including pump, signal and idler waves, were directed and focused by a CaF_2 lens with f = 150 mm towards the mid-IR detector. Then the three beams were passed through a 1 mm thick Anti-Reflecting-coated Germanium filter which absorbed the pump and signal waves with shorter wavelengths while letting the idler wave pass, which was used to separate the infrared light from short wavelengths. The idler wave was subsequently detected by a liquid-nitrogen cooled InSb detector (Hamamatsu Photonics K.K.) with a 3.14 mm^2 active area. The detectivity and the bandwith of the detector are $4.45\times10^{10} cm\cdot\sqrt{Hz}/W$ and 120 Hz, respectively. After detected, the mid-IR signal was transferred into electrical signal and shown on the computer, which was used to control and record the whole process. Since the mid-IR signal was relatively week, which was in the order of micro watt, a pre-amplifier was used.

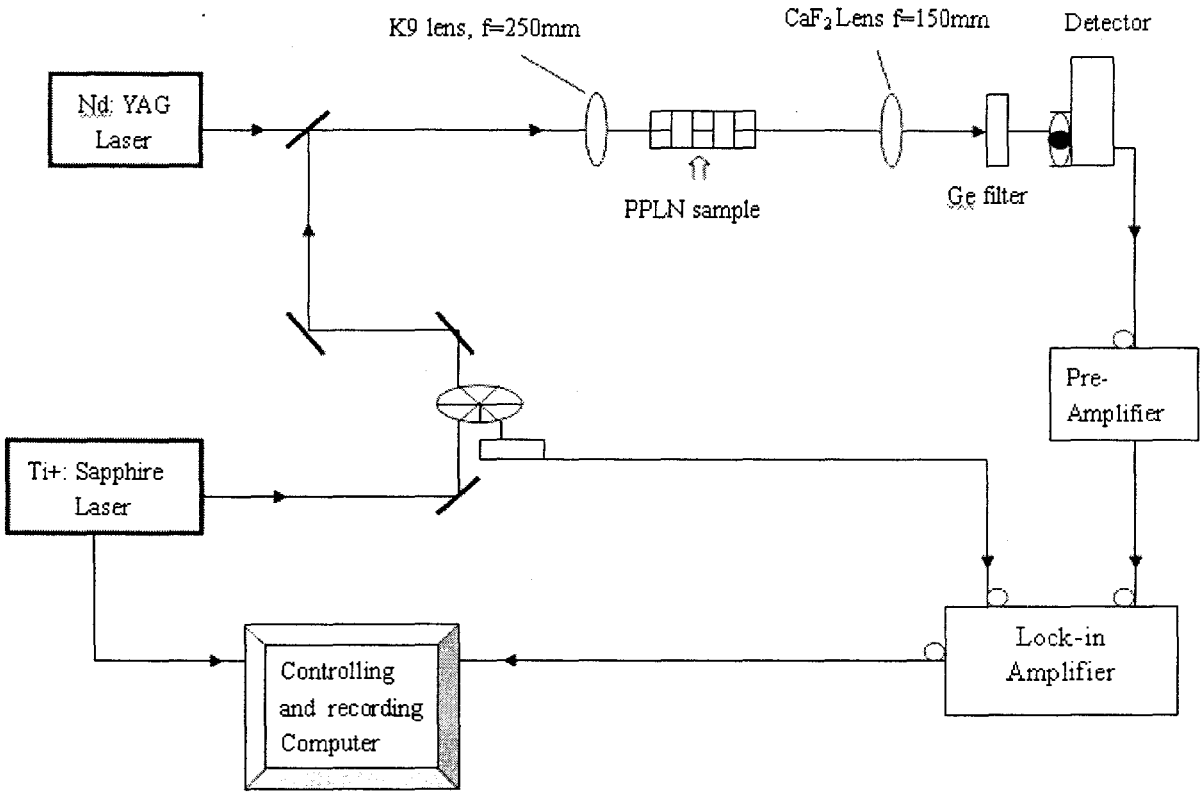

Fig. 4.1 Schematic diagram of the DFG experimental setup

To study the DFG mid-IR laser source in PPLN crystals discussed above, PPLN crystal samples were prepared with two different periods, 22.7 μm and 22.9 μm, by employing the electrostatic crystal poling technique, as described in chapter 3 [1]. The PPLN samples have a dimension of 40 x 9 x 0.5 mm^3. Mid-IR generation from these bulk PPLN crystals was tested.

4.2 Experimental results

4.2.1 Frequency tuning and QPM characteristics

The QPM tuning characteristics have been investigated for the PPLN crystals of the grating period of 22.9 μm and 22.7 μm. In Fig. 4.2, the QPM tuning profiles at different temperatures of the crystal of grating period of 22.9 μm are shown. The tuning lines are plotted as a function of the wavelength of the idler laser, which is in the spectroscopic region of mid-IR. In the experiment, the temperature of the PPLN crystal was tuned starting from 30 °C with the increment of around 10 °C. At each temperature, the wavelength of the pump laser was tuned around the QPM points to get the tuning profiles. According to the Sellmeier equation in Ref. [2], two QPM peaks can be achieved at one temperature when the signal laser is fixed at 1.064 μm and the pumping laser (and thus the generated mid-IR) is tuned. The generated frequency can be tuned from 3.9 μm to 4.5 μm when the temperature of the PPLN crystal increases from 30 °C to 62 °C.

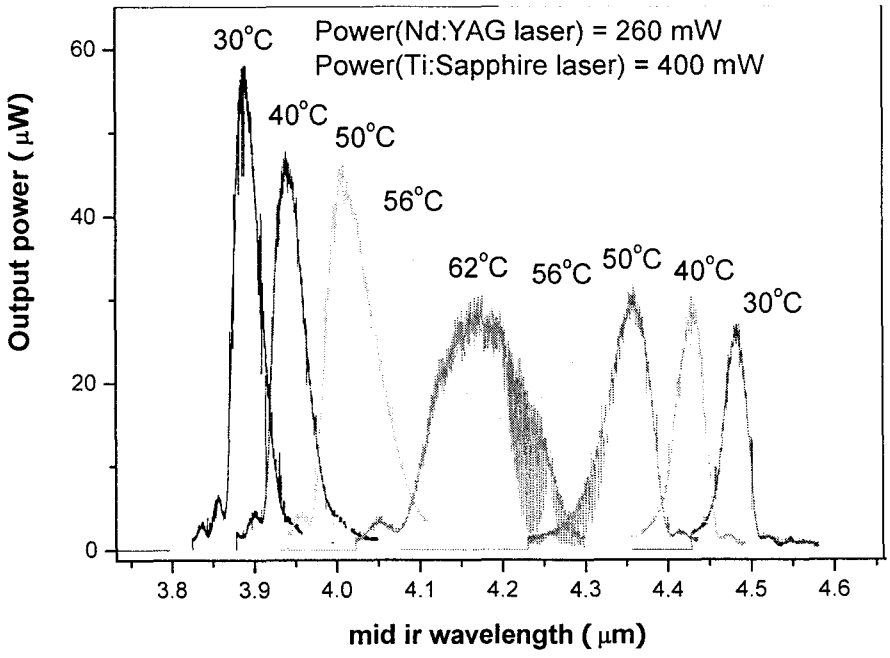

Fig. 4.2 QPM tuning profiles at different temperatures of the PPLN crystal of grating period of 22.9 μm

Similarly, in Fig. 4.3, the QPM tuning profiles at different temperatures of the crystal with a grating period of 22.7 μm are shown. The temperature was tuned from 37 °C to 120 °C, with the increment of 20 °C. The generated frequency can be tuned from 3.9 μm to 4.5 μm. The detailed analysis of the temperature tuning characteristics of PPLN crystal will be studied later in chapter 5.

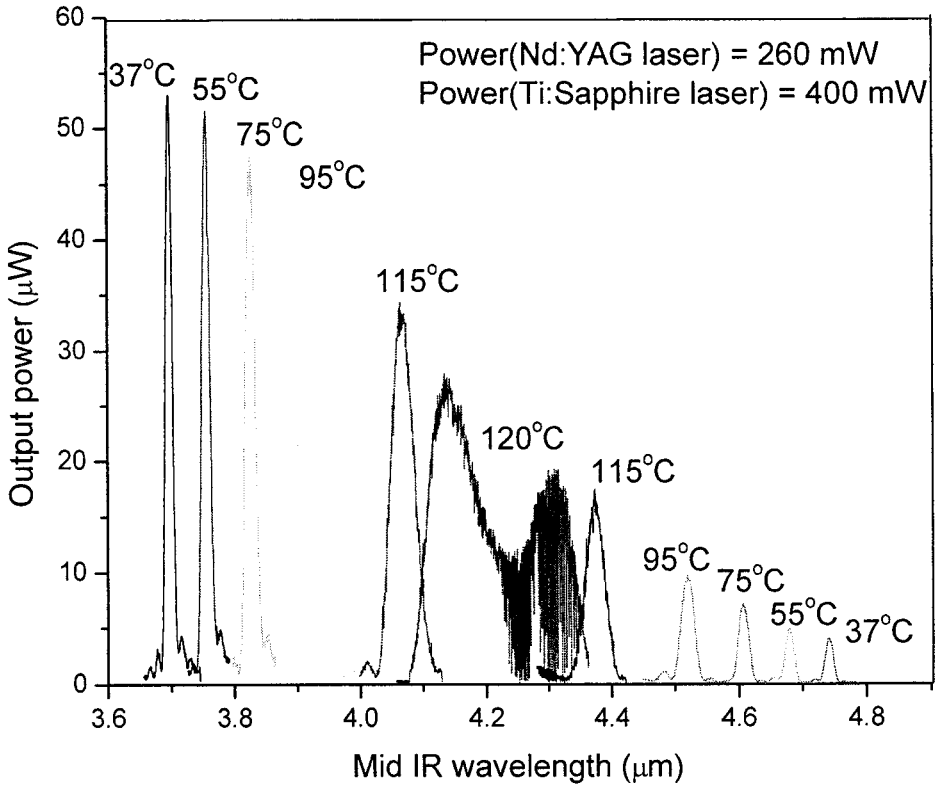

Fig. 4.3 QPM tuning profiles at different temperatures of the PPLN crystal of grating period of 22.7 μm

4.2.2 Output power efficiency estimation

In recent years, based on significant works done by different investigators, higher and higher efficiency of DFG in bulk PPLN has been reported. For example, in Ref. 3, maximum IR power of 12 μW, with 80 mW and 710 mW incident on the crystal from the slave laser and the Nd:YAG laser, respectively was reported. This result translated into an efficiency of 0.021%/W, which compared well with their previous results (0.010%/W) at this wavelength. The theoretical limit was 24 μW (0.042%/W efficiency), calculated from the relation given in the paper, with d_{eff} = 14 pm/V and taking into account the Fresnel reflection losses from crystal surfaces, 13.8%, 13.4%, and 11.8 %, respectively, for 850 nm, 1064 nm, and 4.25 μm beams. They attributed the discrepancy between experimental and calculated efficiency to a non-optimized focusing for input beams. Moreover, they also thought that the duty cycle of the poling period was not precisely 50%, which would also reduce the efficiency of the non-linear mixing [3]. And, a power conversion efficiency of ~ 0.05 %/W cm^{-1} was achieved by F.K. Tittel, etal. at room temperature [4]. Around the same time, radiation of 7 μW at 3.3 μm was generated by mixing a 500 mW DFB diode laser at 1066nm and an erbium doped fiber amplified 1574 nm DFB diode laser in PPLN [5]. In Ref. 6, typical idler power was of the order of 5 μW, resulted from 60mW and 300 mW of the pump and signal power, respectively. This corresponded to a conversion efficiency of 0.0146 %/W cm-1 [6]. In Ref. 7, Mid-IR radiation at 3.36 μm with power ~18 μW was produced by YAG laser at 1064 nm, 220 mW, and a fiber pigtailed DFB diode laser operating at 1560 nm, 50 mW, which corresponded to the efficiency of up to

0.163 %/W [7].

In our work, as plotted in Fig. 4.2 and Fig. 4.3, the generated mid-IR powers with DFG in a 40 mm-long PPLN bulk crystal at different temperatures are between 25 μW and 58 μW. For the data in this figure, the pump and signal laser powers are 400 mW and 260 mW, respectively. So the efficiency of around: 0.048%/W can be achieved. If consider the length of the device, it is ~0.01 %/W cm^{-1}. This efficiency has taken account the reflection losses at the surfaces of the crystal (1%), the loss through the Ge filter (60%) and the loss of the CaF_2 lens (8%). The efficiency can further be enhanced by reducing beam diameter and increasing overlay of the pump and signal beams.

4.2.3 Wavelength acceptance bandwidth

Wavelength acceptance bandwidth has been studied at different PPLN crystal temperatures. Figure 4.5 (a) – (f) show the QPM idler wavelength bandwidths at room temperature (37 °C), 55 °C, 75 °C, 95 °C, 115 °C and 120 °C, respectively. It can be stated from Fig. 4.4 that, at room temperature, a QPM pump wavelength tuning Full Width at Half Maximum (FWHM) of about 0.61 nm has been observed.

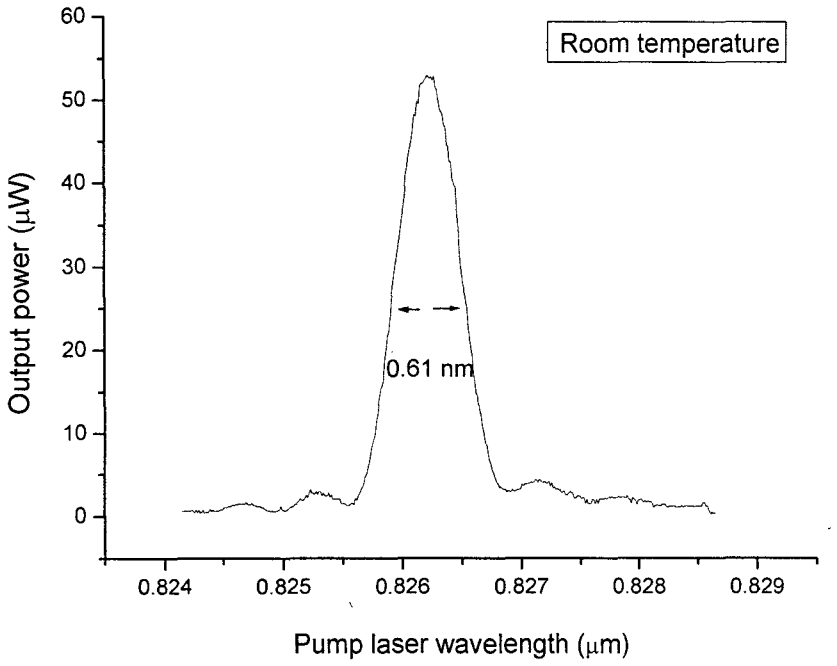

Fig. 4.4 Pump wavelength tuning curve of PPLN sample of the period of 22.7 μm at room temperature (37 °C)

However, the QPM bandwidths are different at different temperature values. It can be seen from Figs. 4.5 (a) – (f) that the QPM bandwidth increases according to the

rising of the temperature of the PPLN crystal. As it can be seen, at room temperature, the bandwidth of idler wavelength is 13 nm , 15 nm, 19 nm, 31 nm, 44 nm at 55 °C, 32 °C , 75 °C, 95 °C, 115 °C, respectively. It's worth noting that, when temperature keeps rising, two QPM peaks will combine together, which results in an extremely broad tuning range, which is shown in Fig.4.5 (f). It's also worth noting that the spectral lines on the tuning curve show the spectrum of the v_3 absorption band of carbon dioxide, which is studied in 4.2.4. As well, the temperature characteristics will be discussed further in chapter 5. When the grating period and temperature are fixed, a detailed study shows that the wavelength acceptance bandwidth would proportion to the value of $d\lambda_p / d\Lambda$, where Λ is the grating period.

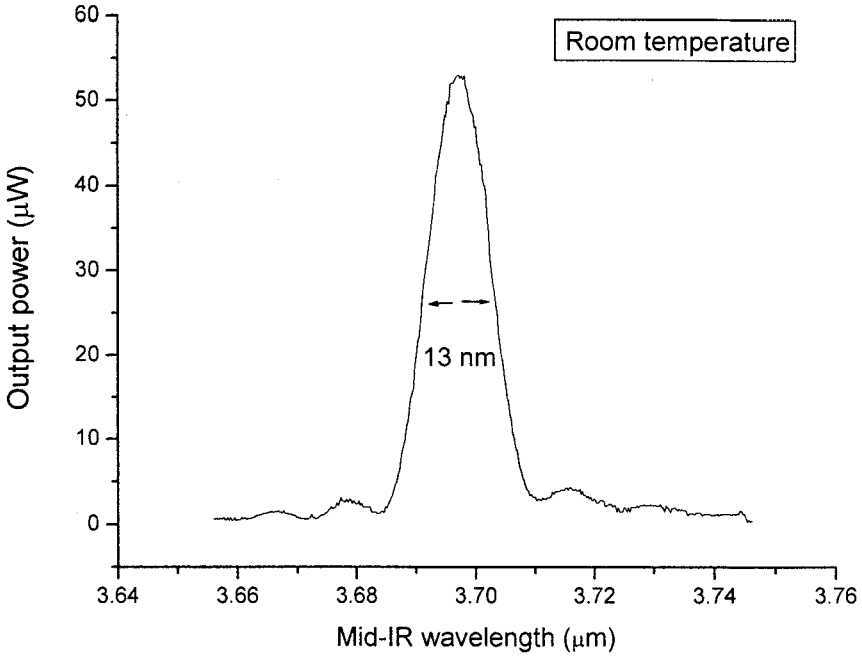

Fig. 4.5 (a) Idler wavelength tuning curve of PPLN of the period of 22.7 μm at room temperature (37 °C)

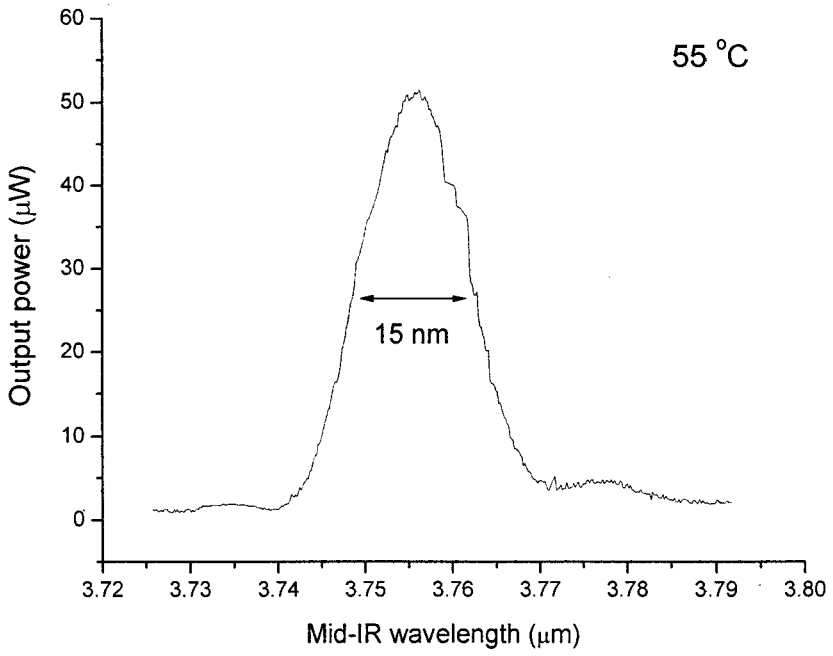

Fig. 4.5 (b) Idler wavelength tuning curve of PPLN of the period of 22.7 μm at 55 °C

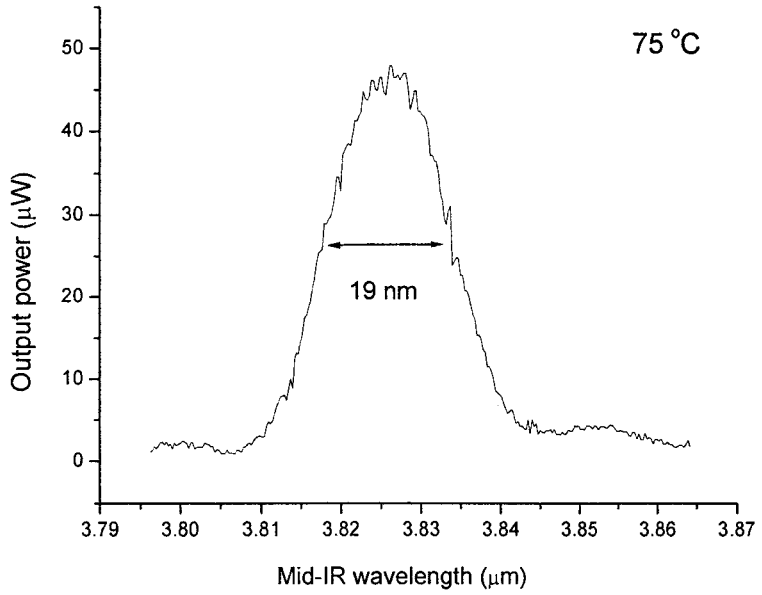

Fig. 4.5 (c) Idler wavelength tuning curve of PPLN of the period of 22.7 μm at 75 °C

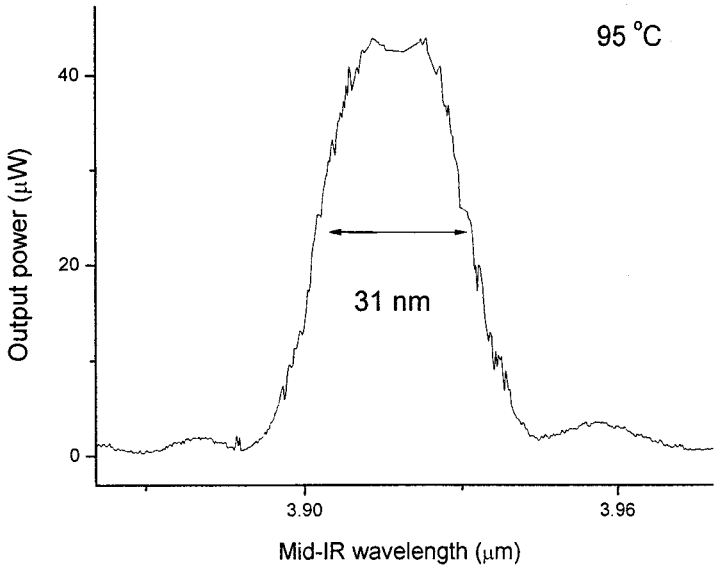

Fig. 4.5 (d) Idler wavelength tuning curve of PPLN of the period of 22.7 μm at 95 °C

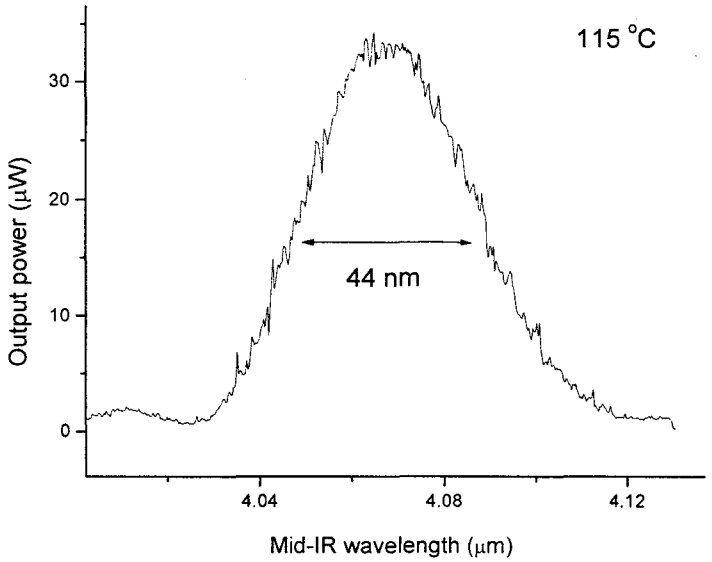

Fig. 4.5 (e) Idler wavelength tuning curve of PPLN sample of the period of 22.7 μm at 115 °C

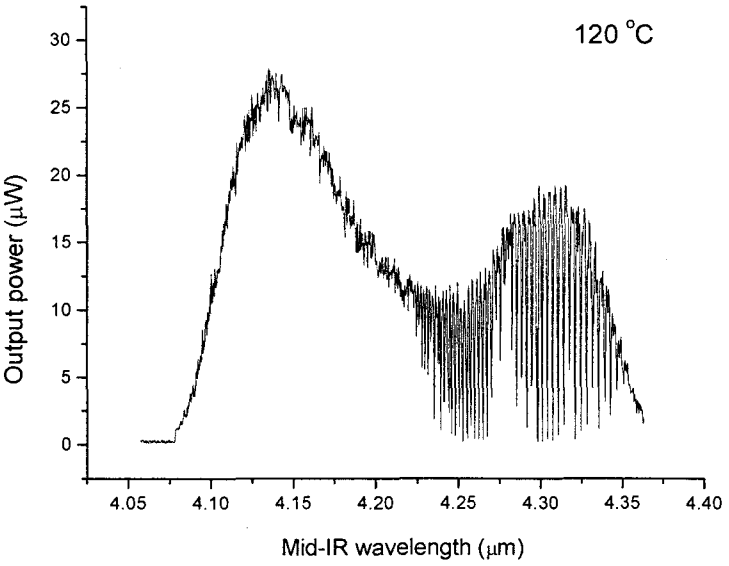

Fig. 4.5 (f) Idler wavelength tuning curve of PPLN sample of the period of 22.7 μm at 120 °C

4.2.4 Spectral characteristics

The absorption spectrum measurement of carbon dioxide near 4.2 μm will be discussed briefly here. Shown in Fig. 4.6 is the ν3 band spectrum of carbon dioxide (CO_2) in open air through about 10 cm optical path between the crystal and the detector [8, 9]. The signal laser was fixed at 1064 nm and the pump laser wavelength was scanned around 850 nm. The grating period was 22.9 μm and the temperature was fixed at 62 °C.

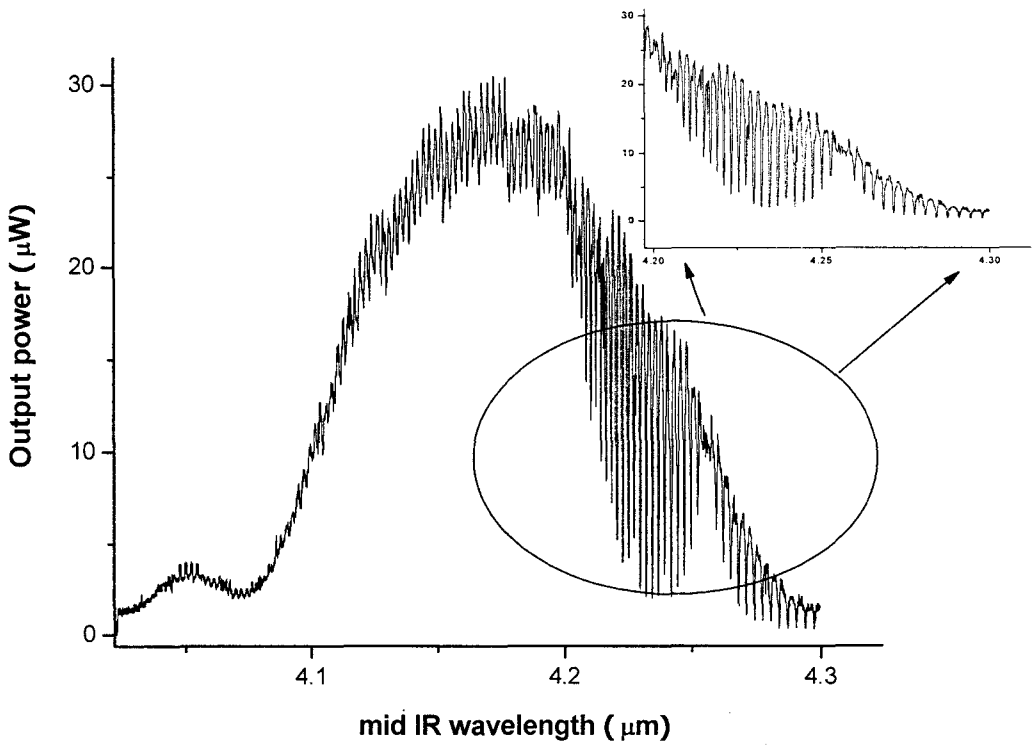

Fig. 4.6 The absorption spectrum measurement of carbon dioxide near 4.2 μm with PPLN crystal of grating period 22.9 μm at 62 °C

In Fig. 4.7, the absorption lines of CO_2 can also be observed in the tuning curve of another PPLN sample of which the grating period was 22.7 μm and the temperature was fixed at 120 °C. The data of the absorption spectrum of CO_2, can be compared with the standard spectrum from HITRAN04 database [10]

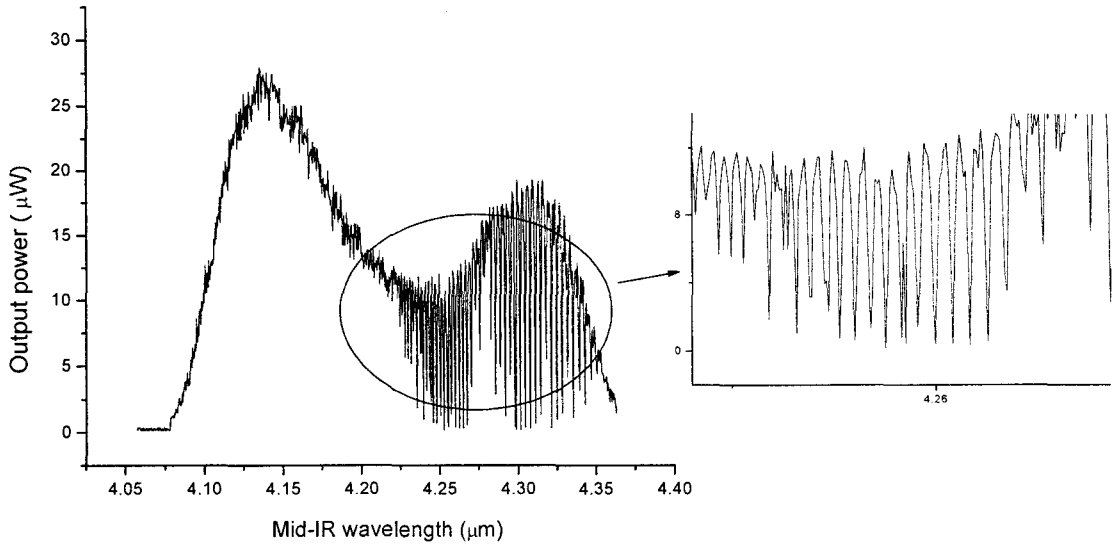

Fig. 4.7 The absorption spectrum measurement of carbon dioxide near 4.2 μm with PPLN crystal of grating period 22.7 μm at 120 °C

In the application of gas detection, the DFG linewidth is of great importance that it determines the selectivity of the system. Generally speaking, the DFG linewidth is mainly determined by the linewidth and frequency stability, including transient center frequency drift, of pump and signal lasers. The linewidth broadening of DFG in the experiment may be caused by transient power shift and central frequency shift of DFG light sources during data acquirement.

The DFG linewidth is estimated to be of several MHz or more, which is

sufficiently narrow for trace gas detection of small molecular species to investigate Voigt or Lorentizian lineshapes whose widths are of several hundred of MHz or more. The DFG system with linewidth of tens of MHz can achieve sufficient spectra selectivity as well. Therefore, the sharp linewidth property is one of the advantages of DFG compared with other techniques.

4.3 Theoretical analysis of QPM wavelength tuning

4.3.1 Modified Sellmeier equation

An improved Sellmeier equation [11] has been reported based on experimental results. The modified equation provides a better fit to present experimental data, and so the simulations in this work also use this new equation given by

$$n_e^2 = a_1 + b_1 f + \frac{a_2 + b_2 f}{\lambda^2 - (a_3 + b_3 f)^2} + \frac{a_4 + b_4 f}{\lambda^2 - a_5^2} - (a_6 + b_5 f)\lambda^2 \qquad (3)$$

$$\begin{aligned} f &= (T - T_0)(T + T_o + 2 \times 273.16) \\ &= (T - 24.5^o C)(T + 570.82) \end{aligned} \qquad (4)$$

where, n_e is the extraordinary refractive index in lithium niobate, λ is the wavelength of the generated light, and T is the operating temperature. The best fitting parameters included in the equation are all given in Table 4.1.

Table 4.1. Best fitting parameters used in modified Sellmier equation [10]

Parameter	Value
a_1	5.35583
a_2	0.100473
a_3	0.20692
a_4	100
a_5	11.34927
a_6	1.5334×10^{-2}
b_1	4.629×10^{-7}
b_2	3.862×10^{-8}
b_3	-0.89×10^{-8}
b_4	2.657×10^{-5}
b_5	9.62119×10^{-10}

4.3.2 Simulation analysis of frequency tuning at different temperatures

As to the theory and equations studied in chapter 3, a calculated relation between the output power of idler laser and the product of the power of signal and pump lasers can be achieved in Fig. 4.8 at different laser beam effective cross sectional areas: A_{eff}.

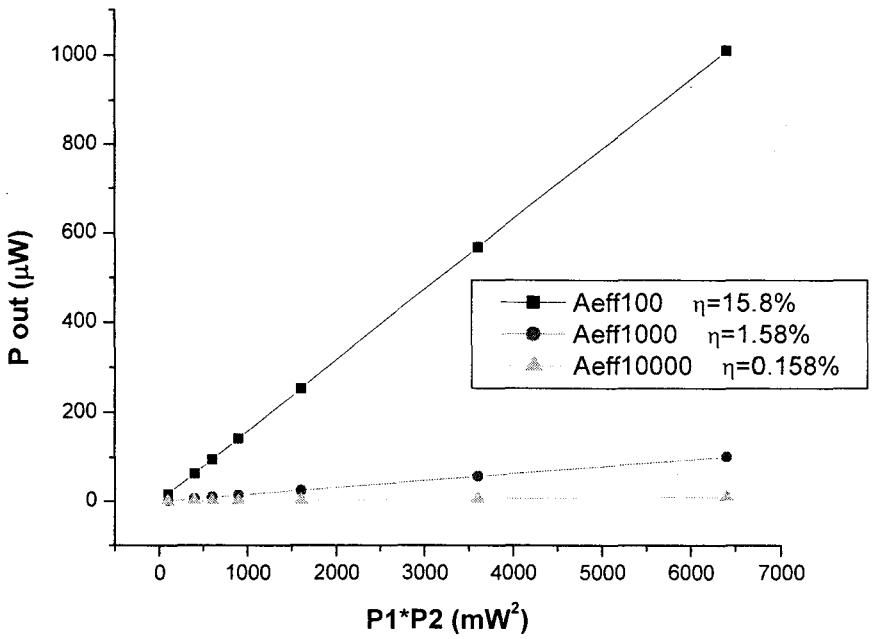

Fig. 4.8 Calculated output power of idler laser depending on the product of the two input powers

If assumeing the A_{eff} is 100 μm, the efficiency is about 15.8 %/W. If we consider the length of the device which is 4cm, we get efficiency is 3.95 %/W cm. (or say 39.5mW/W^2 cm). If the A_{eff} is 1000, the efficiency is 0.395%/W cm, which is in proportion by inversion with the cross section value. The comparison of the simulation and the experimental results will be discussed in Chapter 5.

Fig. 4.9 shows the wavelength dependence of the simulated output power of the mid-IR light generated by a PPLN crystal with a period of 22.9 μm at different temperatures. The simulations were obtained by using the theories and equations in chapter 3 and the Sellmeier equation given above. In the simulations, the signal

wavelength and device length were fixed at 1.064 μm (with an input power of 100 mW), and 40 mm, respectively; the pump wavelength was tuned from 800 nm to 860 nm at a constant power of 100 mW. The dependence of the output power on temperature (which was set to 30 °C, 40 °C, 50 °C, 56 °C, and 62 °C in the simulation) arises from the Sellmeier equation. Laser beam effective cross sectional areas, A_{eff}, of 100 μm^2 and effective nonlinear optical coefficient, d_{eff}, of 0.02 nm/V were used in the simulations. Under these conditions, the calculated output power of the mid-IR light is around 1.5 mW. It is worth noting that using the same value of effective cross sectional area for all the three beams involved in the DFG process might not be realistic since the generated mid-IR wavelength is quite different from the input beams, but this will not have a significant impact in the analysis of wavelength tuning characteristics.

As shown in Fig. 4.9, two peaks can be achieved at one temperature when the signal laser is fixed at 1.064 μm and the pumping laser (and thus the generated mid-IR) is tuned. At temperatures of 30 °C, 40 °C, and 50 °C, double peaks at 3.9 μm and 4.48 μm, 3.95 μm and 4.43 μm, and 4.02 μm and 4.35 μm, respectively, were obtained. The two peaks move closer to each other in wavelength as the temperature is increased, which is an effect that will be explained below. At 56 °C, the peaks begin to overlap and eventually merge into one peak at 62 °C. When the temperature is above 62 °C, 65 °C for example, the power of the generated mid-IR light decreases suddenly and reaches an extremely low level. The simulation suggests that broadband mid-IR sources can be achieved over a temperature range of 30 °C - 62 °C. For a

PPLN crystal with a poling period of 22.9 μm, a maximum tuning bandwidth of 580 nm can be achieved by varying the temperature from 30 - 62 °C for coarse adjustments and varying the pump wavelength from 836 nm - 860 nm for fine adjustments.

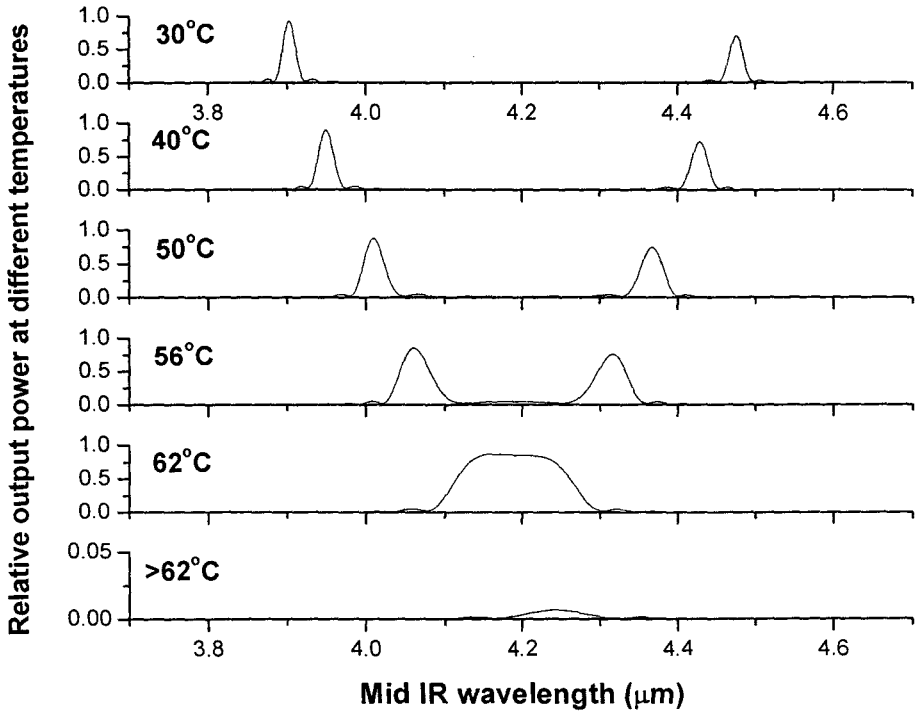

Fig. 4.9 Simulation of pump wavelength tuning of 22.9 μm period crystal at different temperatures.

Similarly, mid-IR wavelength tuning with temperature for a PPLN crystal with a poling period of 22.7 μm was simulated, as shown in Fig. 5.10. This period was chosen so as to match our experimental parameters. Consistent with the results in Fig. 4.3, we obtain two peaks at each temperature covering a wavelength range of 3.7 μm - 4.7 μm by varying the temperature from 30 °C to 120 °C. Thus for a PPLN crystal

with a period of 22.7 μm, a maximum tunable bandwidth of 1000 nm can be achieved by varying the temperature from 30 °C to 120 °C for the coarse adjustments and varying the pump wavelength from 830 to 870 nm for fine adjustments. As studied in this chapter and compared with the experimental results in chapter 6, the simulations agree well with the experimental data.

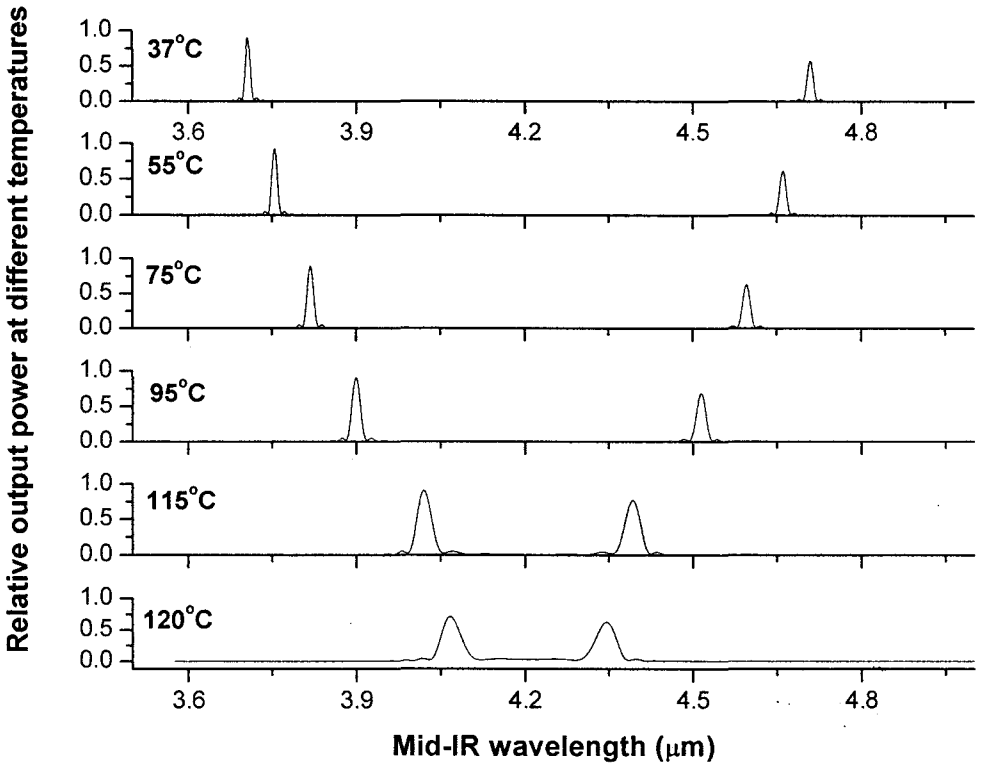

Fig. 4.10 Simulation of wavelength tuning at different temperatures in 22.7 μm period crystal

References for chapter 4

[1]. C.Q. Xu, **invited**, Proc. of The 4th Asia Pacific International Symposium on the Basic and Application of Plasma Technology, 2005, Taiwan, R.O.C., pp.49-53.

[2]. Dieter H, Jundt, Opt. Lett. **22**, 1553-1555 (1997).

[3]. D. Mazzotti, P. De Natale, G.Giusfredi, C. Fort, J.A. Mitchell, L.W. Hollberg, Appl. Phys. B 70, 747–750 (2000) Lasers and Optics

[4]. W. Chen, G..Mouret, D. Boucher, F.K. Tittel, Appl. Phys. B 72, 873–876 (2001) Lasers and Optics

[5]. D.G.. Lancaster, R. Weidner, D. Richter, F.K. Tiottel, J. Limpert, Optics Communications 175 (2000) 461-468.

[6]. D. Mazzotti, P. Cancio, G.. Giusfredi, and P. De Natale, May 1, 2005 / Vol. 30, No. 9 / OPTICS LETTERS

[7]. H.Y. Clark, L. Corner, W. Denzer, G.. Hancock, et. Chemical Physics Letters 399 (2004), 102-108.

[8]. W. Chen, G. Mouret, D. Boucher, F.K. Tittel, Appl. Phys. B **72**, 873 (2001)

[9]. Mazzotti D., De Natale P., Giusfredi G., Fort C., Mitchell J.A., Hollberg L.W. Opt. Lett. **25**, 350 (2000)

[10]. L.S.Rothman, D. Jacquemart, A. Barbe, D.C. Benner, M. Birk, L.R. Brown, M.R. Carleer, C. Chackerian, Jr, K. Chance, V. Dana, V.M. Devi, J.M. Flaud, R.R. Gamache, A. Goldman, J.M. Hartmann, K.W. Jucks, A.G. Maki, J.Y. Mandin, S. Massie, J. Orphal, A. Perrin, C.P. Rinsland, M.A.H. Smith, R.A. Toth, J. Vander Auwera, P.

Varanasi, G. Wagner, Journal of Quantitative Spectroscopy and Radiative Transfer **96**, 139 (2005)

[11]. L.H. Deng et al., Optics Communications **268,** 110-114 (2006).

CHAPTER 5:

BROADLY TUNABLE MID-IR LIGHT GENERATION BY TEMPERATURE TUNING OF PPLN DFG DEVICE

5.1 wavelength tenability of DFG in PPLN or other nonlinear crystals

One of the main reasons that the reported mid-IR light generation techniques based on DFG in PPLN or other crystals have attracted special attention is the attractively broad wavelength tunability. For example, a tuning range of 5 – 12 μm has been achieved using difference-frequency mixing in a AgGaS2 crystal [1]. Although this is a broad range, it is not in the 2 – 5 μm region desired for atmospheric gas detection. By using a PPKTP crystal as the DFG medium in an optical parametric oscillator (OPO), mid-IR generation from 4.5 to 4.6 μm was achieved when the temperature was tuned from 25 °C to 200 °C [2]. DFG in PPLN crystals is particularly impressive because of high conversion efficiency, wide thermo-optic tuning range, and high transparency in the entire 2 - 5 μm region. In Ref. 3, light generation from 4 - 4.6 μm was achieved in a PPLN crystal by varying the temperature from 16 °C to 40 °C while simultaneously tuning the Ti^{3+}:sapphire laser (812 - 835nm) at a fixed diode laser wavelength of 1020 nm. In Ref. 4, a bandwidth of ~ 100 nm was achieved by setting the temperature around 26 °C in a multisection temperature-tuned PPLN

device. Despite the prospect of achieving broad band mid-IR generation, these examples illustrate that the exact generation process in PPLN and/or other crystals is not yet fully understood, with questions such as why the reported tunable bandwidths are so different and how to achieve the maximum tunable bandwidth from a single device remain unanswered.

5.2 Optimization of wavelength tunability of DFG in PPLN

In this work, the wavelength tuning characteristics of mid-IR light generation in PPLN crystals are studied both theoretically and experimentally. An effective method to obtain the optimized mid-IR tuning width in a PPLN crystal with a single period is proposed in this chapter. The questions described above can be answered with consistency based on our studies.

Concluding from chapter 4, it is interesting to point out that the maximum tunable bandwidth of the PPLN DFG devices depends strongly on the period of the PPLN crystal. This explains well why the reported tunable bandwidth of the PPLN DFG mid-IR generators is so different in the literature.

To explore if the maximum tunable bandwidth can be further enhanced by optimizing the PPLN device design, wavelength tuning of the generated mid-IR light from a 20.9-μm period PPLN were also simulated, as shown in Fig. 5.1. The device

operating temperature varied from 30 °C to 500 °C. As shown in Fig. 5.1, mid-IR light generation over a range as large as 2800 nm can be achieved by simply tuning the temperature from 30 °C to 500 °C and the pump wavelength from 778 nm to 900 nm. To the best of our knowledge, there have been no reports of a device producing mid-IR generation with a bandwidth this large. It is expected that if the highest device operating temperature is raised, even broader tuning widths can be achieved with proper choice of the PPLN poling period. Based on these simulations, we can thus conclude that wavelength tunable lasers covering the entire mid-IR region of 2 – 5 μm can be realized using a single-period PPLN crystal while tuning the pump wavelength at different temperatures.

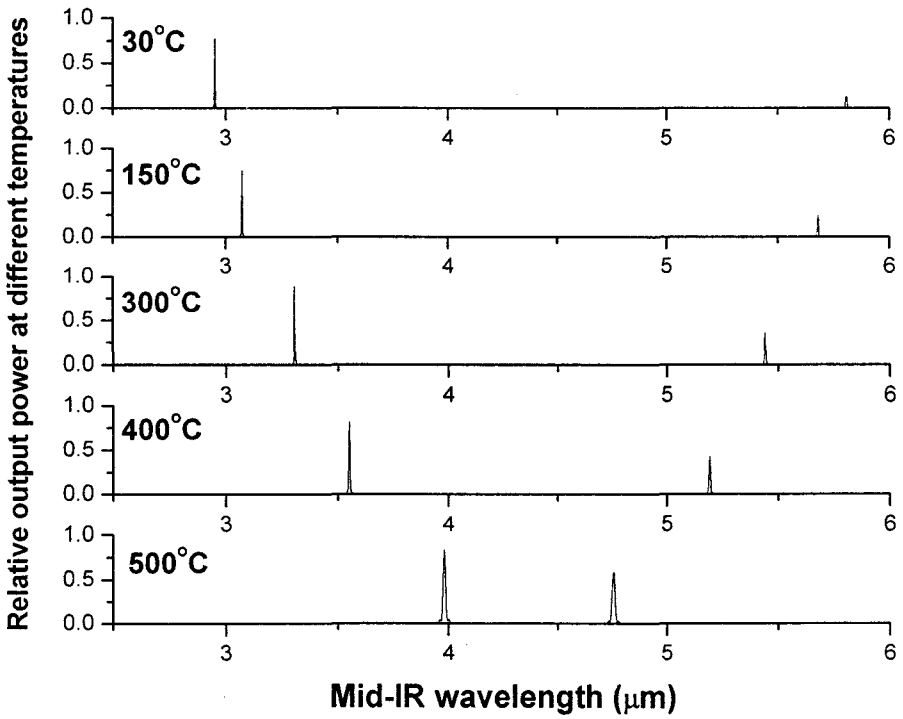

Fig. 5.1 Simulation of temperature tuning of 20.9 μm period crystal.

To aid in the design of maximum tunable bandwidth PPLN devices at given operating conditions (e.g. device temperature), the PPLN period as a function of the QPM wavelength was calculated and plotted in Fig. 5.2 for different temperatures. The shape of the curves clearly indicates that two wavelengths can be generated at each temperature for polling periods less than the curve peaks. If the poling period is kept constant, increasing the temperature causes the two matching points to move closer to each other until they finally merge to one point at a temperature corresponding to the peak of the curve. This explains well why we can usually obtain two peaks at one temperature as in Fig. 4.2 and Fig. 4.3. Further increasing the temperature, while keeping the poling period constant, results in no intersection of the two curves and thus QPM is not satisfied. This can explain why the generated mid-IR light power decreases suddenly in Fig. 4.9 when temperature exceeds 62 °C. Using the above observations, we have devised the following procedure for optimization of a PPLN DFG device via the appropriate choice of polling period:

Step 1: Calculate and plot the PPLN polling period vs. generated mid-IR wavelength under the QPM conditions for the highest (e.g. 500 °C) and lowest (e.g. 25 °C) operating temperatures;

Step 2: Draw a horizontal line through the peak of the curve for the highest operating temperature (as shown in Fig.5.2).

Step 3: Obtain the optimized period of the PPLN crystal by finding the cross point of the horizontal line with the Y-axis;

Step 4: Find the tunable bandwidth of the designed PPLN DFG mid-IR generator by taking the difference between the two wavelength intersection points of the horizontal line with the lowest temperature curve.

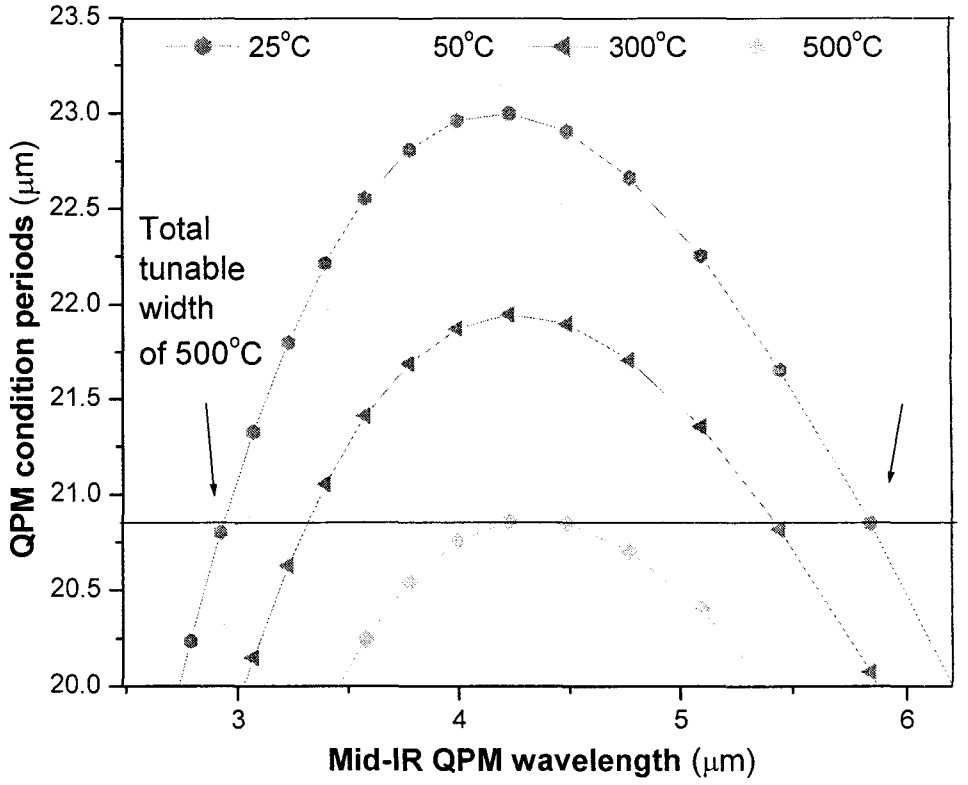

Fig. 5.2 Signal wavelength is fixed at 1.064 μm, and the pump wavelength is tunable from 700 nm to 900 nm. A detailed view of DFG domain periods depending on pump wavelength tuning of PPLN crystal, of which the tuning temperature is from 25 °C to 500 °C and the corresponding crystal periods between 20.9 - 23.0 μm.

From the theoretical simulations, it is apparent that for a large enough temperature range and extremely large generation bandwidth can be obtained in the mid-IR region. In other words, the optimized tunable mid-IR range is determined by

the lowest and highest temperature limits along with the appropriate choice of poling period. From Fig. 5.2 we can see that choosing a poling period of 20.9 μm and a temperature range from room temperature to 500 °C can lead to mid-IR light generation from around 2.9 μm to 5.8 μm, resulting in a bandwidth of 2800 nm.

Fig. 5.3 shows the temperature dependent spectra of the normalized mid-IR light power by a PPLN crystal with a period of 22.9 μm. As can be seen, two peaks were observed at each temperature, and move closer to each other as the temperature is increased, which agrees well with the theoretical simulations based on the Sellmeier equation shown in Fig.5.2. A tunable range of about 800 nm was achieved from this device when the operating temperature was tuned from 30 °C to 62 °C, which matches the simulations exceptionally well.

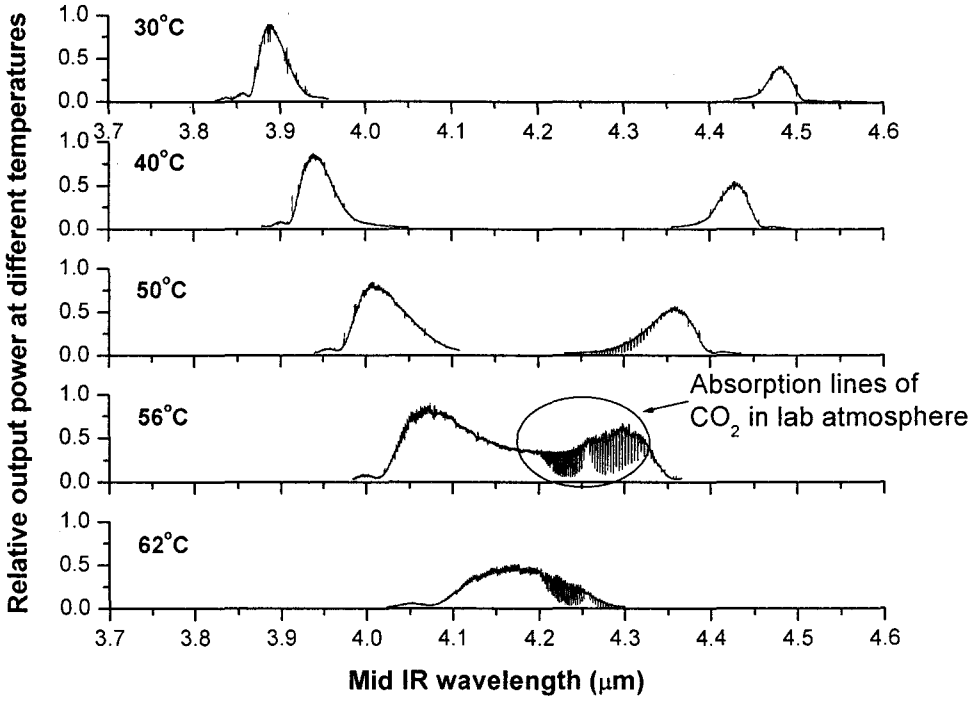

Fig. 5.3 Experiment result of pumping wavelength tuning in PPLN crystal with a period of 22.9 μm.

Fig. 5.4 shows the temperature dependent spectra of the normalized mid-IR light power by a PPLN crystal with a period of 22.7 μm. Mid-IR light with a tunable range as large as 1000 nm can be achieved by simply varying the temperature from 37 °C to 120 °C for coarse tuning and varying the Ti:sapphire pump laser wavelength for fine adjustments.

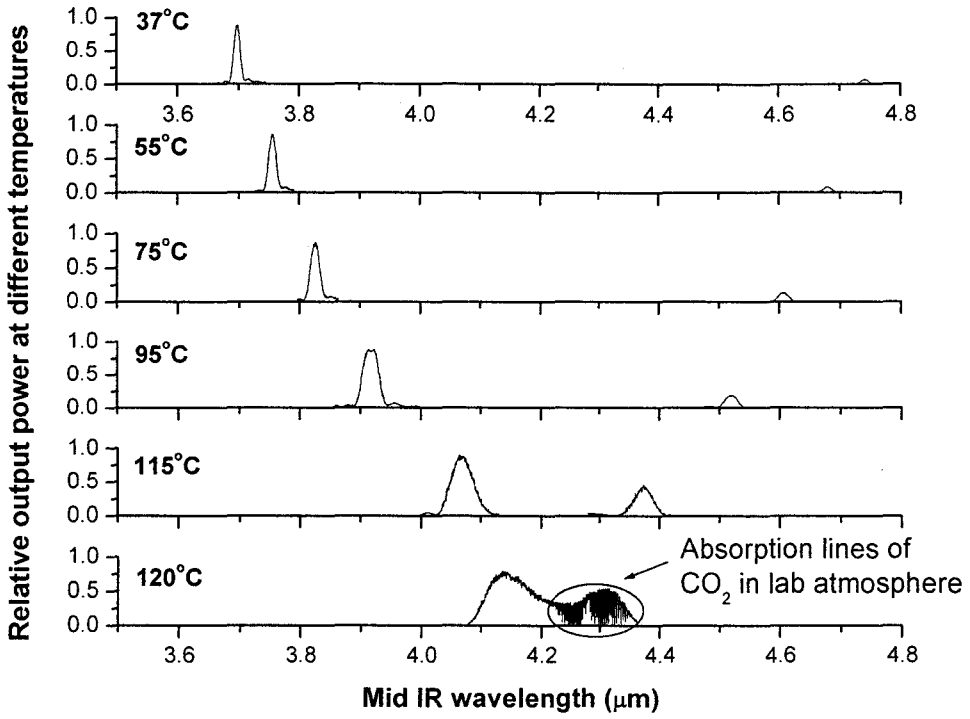

Fig. 5.4 Experiment result of temperature tuning in PPLN crystal with a period of 22.7 μm.

Figure 5.5 shows the maximum mid-IR tunable bandwidth as a function of the highest device operating temperature (dashed line). For comparison, the measured and reported data (black squares) are shown on the same plot. As shown in the figure, our simulation results based on the optimization procedure described above agree very well with the experimental data, implying that the tunable bandwidth optimization method presented in this paper is very effective for the design of widely tunable mid-IR lasers based on the DFG technique.

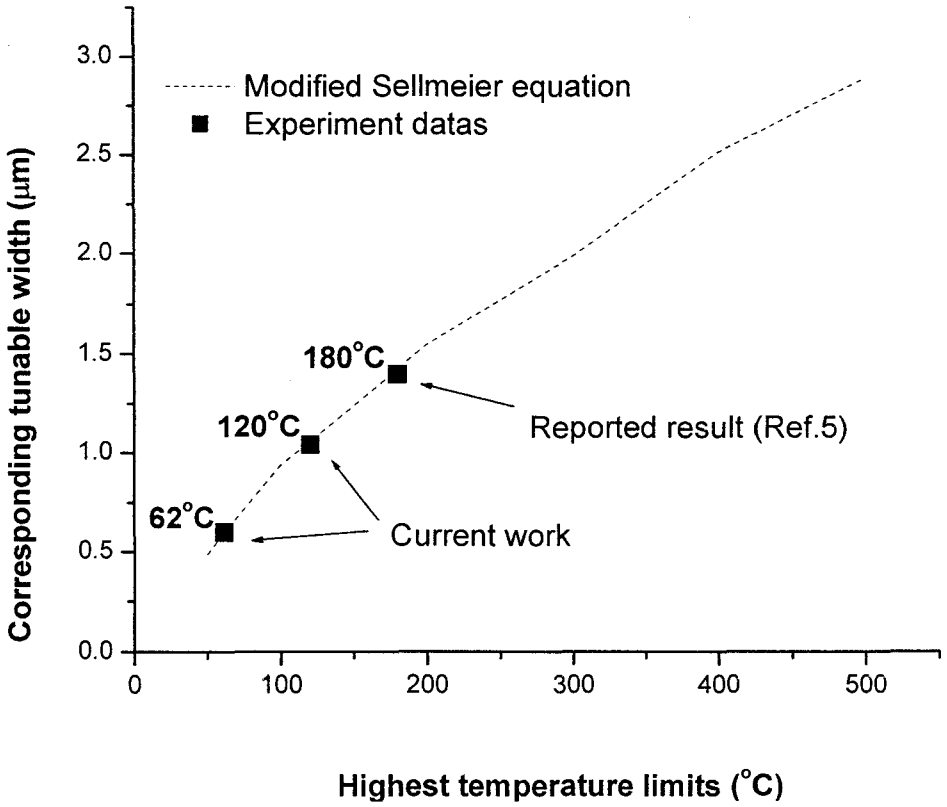

Fig. 5.5 DFG Mid-IR tunable width corresponding to the highest temperature limits in reported and current works

References for Chapter 5

[1]. S Haidar, E Niwa, K Masumoto and H Ito, J. Phys. D: Appl. Phys. **36,** 1071–1074 (2003).

[2]. Wei Quan Zhang, Optics Communications **252**, 179 - 187 (2005).

[3]. Nilesh J. VASA, Husayin PARHAT, Masahiro KIDOSAKI, Tatsuo OKADA, Mitsuo MAEDA, Hirokazu TANAGUCHI, Masaru NAKAMURA, Pacific Rim'99 CLEO WG4, pp. 181-182 (1999).

[4]. Xuefeng Tang, Zongyan Wu, and Paul Urquhart, Journal of Lightwave Technology **22**, 1622-1627 (2004).

[5]. L.H Deng, X.M Gao, Z.S Cao, Y.Q Yuan, Z.B Gong, submitted to Applied Physics B: Lasers and Optics (Private communication, 2007)

CHAPTER 6: CONCLUSION

6.1 Main contributions of this work

The objective of this work was to develop a broadly tunable mid-IR laser source based on QPM DFG in bulk PPLN crystals. In conclusion, main contributions of this project are as followed.

An important question that needs to be answered when considering using the mid-IR source in gas detection applications is how large wavelength range it can be tuned over. Because in the applications of trace gas detection it's really desired that the mid-IR source can cover most of the wavelength range of the absorption spectroscopy of all the trace gases in the atmosphere. With this in mind, we have proposed a method to gain ultra-broadly tunable mid-IR laser source based on a single device of bulk PPLN when the operating temperature of the crystal is tunable.

In the work, a widely tunable laser source of wavelength 2 to 5 μm was achieved by directly mixing two near infrared lasers as pump and signal sources in a bulk PPLN crystal.

A widely tunable mid-IR laser source based on Difference frequency generation in bulk PPLN crystals was studied in chapter 5. The experimental performances of the DFG laser source in bulk PPLN were studied. It was observed that the wavelength tuning could cover most of the 2 - 5 μm spectral region. By

analyzing the tunable mid-Infrared laser theoretically and experimentally, the characteristics of the nonlinear crystal lithium niobate and DFG based laser sources have also been described and concluded.

An optimization procedure to achieve the maximum tunable bandwidth from PPLN crystal with a fixed period has been proposed and verified by experimental results in chapter 6. It has been found that the maximum tunable bandwidth of the generated mid-IR laser is mainly determined by the period of the PPLN crystals, which should be decided by the highest and lowest device operating temperature. The simulated tunable bandwidth of the generated mid-IR light agrees well with experimental observations. It is shown from the simulations that for a PPLN crystal with a fixed polling period of 20.9 μm, mid-IR light with a tunable bandwidth as large as 2800 nm can be generated by varying the crystal temperature from 25 to 500 °C and the pump laser wavelength from 778 nm to 900 nm while the signal wavelength is fixed at 1.064 μm. We suggest that the optimization procedure of achieving maximum tunable bandwidth can also be applied to DFG devices based on other materials such as PPKTP.

The absorption of CO_2 gas in the open atmosphere in the lab was observed in the tuning curves around 4.2 μm, which is a good start to discuss the application of mid-IR source we achieved in gas detection.

6.2 Discussion and future work

Besides the results achieved so far, there are still lots of improvements need to be done about the design and experiment processes. Since the output power efficiency is one of our most important concerns in the experiment, it is not yet satisfying and lots of work should be done to improve it.

The following improvements are recommended for the PPLN based QPM DFG mid-IR laser sources:

PPLN waveguide can be used instead of bulk crystals to reduce losses and to increase frequency conversion efficiency of the DFG based mid-IR output.

In bulk PPLN crystals and waveguides, optical damage can be an important problem for DFG process since the high-power optical source is used. To reduce this problem, doping of optical-damage-resistant ions (Mg^{2+}, Zn^{2+}, In^{3+}, Sc^{3+}, Hf^{4+}, and Zr^{4+}) in the lithium niobate crystal can be employed. So, in our future work, MgO doped PPLN crystals instead of pure lithium niobate will be used.

Anti-reflection coated samples could also be employed.

As to the applications of the laser source, it will be part of our main future works. The absorption of other gas types will be tested in future and discussed in detail.